

SOME THEORETICAL IMPLICATIONS
OF STRIKE-SLIP FAULTING

by

JOHN A. PETRAK

B.Sc., University of British Columbia, 1964

A THESIS SUBMITTED IN PARTIAL FULFILMENT OF
THE REQUIREMENTS FOR THE DEGREE OF
MASTER OF SCIENCE
in the Department
of
GEOPHYSICS

We accept this thesis as conforming to
the required standard:

THE UNIVERSITY OF BRITISH COLUMBIA

September 1965

In presenting this thesis in partial fulfilment of the requirements for an advanced degree at the University of British Columbia, I agree that the Library shall make it freely available for reference and study. I further agree that permission for extensive copying of this thesis for scholarly purposes may be granted by the Head of my Department or by his representatives. It is understood that copying or publication of this thesis for financial gain shall not be allowed without my written permission.

Department of Geophysics

The University of British Columbia
Vancouver 8, Canada

Date February 2, 1966

ABSTRACT

When a fault occurs in the earth's crust, the ground in its vicinity becomes deformed. This thesis uses the theory of dislocations, as developed by J. A. Steketee, to examine the nature of this deformation for a variety of strike-slip fault models.

The theory is developed for calculating the displacement field and stress changes expected at any point around a vertical transcurrent dislocation surface whose net displacement is constant in the horizontal direction, and varies with depth. The results obtained are compared graphically with geodetic data, and those discrepancies that arise between theory and observation are attributed to the limiting assumptions of the model. The principal conclusion of this work is that the variable-slip fault model provides a significant improvement over previous fault models which assumed a constant displacement.

ACKNOWLEDGMENTS

The author wishes to express his gratitude to Professor M. A. Chinnery, on whose work this thesis is based, and whose suggestions and helpful discussions have been most valuable.

Thanks are also due to Dr. J. A. Jacobs, Head of the Department of Geophysics, U.B.C., who accepted the writer into his group and provided sufficient National Research Council funds to carry out this project.

TABLE OF CONTENTS

	Page
ABSTRACT	ii
ACKNOWLEDGMENTS	iii
TABLE OF CONTENTS	iv
LIST OF ILLUSTRATIONS	vii
LIST OF TABLES	ix
INTRODUCTION	1
CHAPTER 1 HISTORICAL REVIEW	3
1.1 The Concept of Fracture	3
1.2 Application of Fracture to Geology	4
1.3 Basic Assumptions of Dislocation Theory	6
CHAPTER 2 THE DISPLACEMENT FIELD AND STRESS CHANGES DUE TO A RECTANGULAR DIS- LOCATION WITH VARIABLE SLIP	8
2.1 The Equations of Elasticity	8
2.2 The Basic Equations	9
2.3 Galerkin Vectors	11
2.4 The Galerkin Vectors for the Displace- ment Field	13
2.5 Integration over the Dislocation Surface	14
2.6 Expressions for the Stress Change	17
2.7 The Maximum Shear Stress	22

CHAPTER 3	COMPUTATION OF THE DISPLACEMENTS AND STRESS CHANGES PRODUCED BY VARIOUS FAULT MODELS	25
3.1	The Basic Model	25
3.2	Evaluation of the Integrals Using Numerical Procedures	28
3.3	Computation of the Displacements and Stresses	30
3.4	Plotting of the Displacements	31
3.5	Horizontal Displacements	32
3.6	Perpendicular Displacements	38
3.7	Vertical Displacements	39
3.8	Plotting of the Stress Changes and Maximum Shear Stress	39
3.9	Results of the Horizontal Displacement Analyses	40
3.10	Results of the Stress Analyses	52
CHAPTER 4	A COMPARISON OF THE THEORETICAL DISPLACEMENT FIELD WITH OBSERVATIONS	55
4.1	The Source of Geodetic Data	55
4.2	The San Francisco Earthquake	56
4.3	The Tango Earthquake	57
4.4	The North Izu Earthquake	57
4.5	The Imperial Valley Earthquake	58
4.6	The Nevada Earthquake	59
4.7	Application of Theory to Observation	65
4.8	Interpretation of the Fall-off Curves	67

CHAPTER 5	A COMPARISON OF THE THEORETICAL STRESS DISTRIBUTION WITH OBSER- VATION	70
5.1	The Geodetic Data	70
5.2	The Relationship Between the After- shock Zone and Maximum Shear Stress	72
CHAPTER 6	CONCLUSIONS	78
APPENDIX	THE EVALUATION OF THE DISPLACEMENT FIELD AND THE STRESS CHANGES	81
APPENDIX A	THE DISPLACEMENT FIELD	83
APPENDIX B	THE STRESS CHANGES	92
APPENDIX C	THE MAXIMUM SHEAR STRESS	96
REFERENCES		98

LIST OF ILLUSTRATIONS

FIGURE NO.		Page
2.1	Dimensions of the Model	18
3.1	Displacement u_1 in the Plane $y_1 = 0$ (Chinnery)	33
3.2	Displacement u_1 in the Plane $y_1 = 0$ (Model A)	34
3.3	Displacement u_1 in the Plane $y_1 = 0$ (Model B)	35
3.4	Displacement u_1 in the Plane $y_1 = 0$ (Model C)	36
3.5	Fall-off of u_1 with y_2 along $y_1 = y_3 = 0$ (for various models)	37
3.6	Stress Component τ_{12} in the Plane $y_1 = 0$ (Model A)	41
3.7	Stress Component τ_{13} in the Plane $y_1 = 0$ (Model A)	42
3.8	Stress Component τ_{12} in the Plane $y_1 = 0$ (Model B)	43
3.9	Stress Component τ_{13} in the Plane $y_1 = 0$ (Model B)	44
3.10	Stress Component τ_{12} in the Plane $y_1 = 0$ (Model C)	45
3.11	Stress Component τ_{13} in the Plane $y_1 = 0$ (Model C)	46
3.12	Fall-off of τ_{12} with y_2 along $y_1 = y_3 = 0$ (for various models)	47
3.13	Maximum Shear Stress Magnitudes ($y_1 = 0$, Model A)	48
3.14	Maximum Shear Stress Magnitudes ($y_1 = 0$, Model B)	49

3.15	Maximum Shear Stress Magnitudes ($y_1 = 0$, Model C)	50
4.1	Fall-off of u_1 with distance in the San Francisco Earthquake	60
4.2	Fall-off of u_1 with distance in the Tango Earthquake	61
4.3	Fall-off of u_1 with distance in the North Izu Earthquake	62
4.4	Fall-off of u_1 with distance in the Imperial Valley Earthquake	63
4.5	Fall-off of u_1 with distance in the Nevada Earthquake	64
5.1	Aftershock Sequence of Rat Island Earthquake	73
5.2	The Hypothetical Fault Trace Asso- ciated with the Rat Island Earthquake	73
5.3	Maximum Shear Stress Magnitudes ($y_1 = 0$, Model D)	74
5.4	Maximum Shear Stress Magnitudes ($y_1 = 0.95L$, Model D)	75

LIST OF TABLES

TABLE NO.		Page
4.1	Results of the Model Calculations on Some Real Faults	68
A.1	Table (I) of Relationships	84
A.2	Table (II) of Relationships	85

INTRODUCTION

The object of this thesis is not only to determine the various components of the theoretical displacement field and stress changes that arise when a strike-slip fracture occurs in the earth's crust, but also to apply them to various geological situations.

It is our purpose to discuss some of the aspects of the theory of dislocations which may be of significance in geophysical problems connected with fault plane studies of earthquakes and such phenomena as the San Andreas fault in California. Problems connected with fracture zones in the earth's crust and their corresponding aftershock distributions, as exhibited by the Rat Island earthquake in Alaska, are of particular interest. However, it is evident that a lack of pertinent geological data, among other things, hinders some of our analyses to a considerable extent.

Previous approaches to this problem using dislocation theory (e.g. Chinnery 1962) were made possible only by the efforts of Steketee (1957, 1958a, 1958b). The mathematical techniques that were derived from this theory allow us to calculate the difference between the initial and final states of the medium surrounding the

fault: to be more precise they permit us to calculate only the after-effects of a static fracture situation.

As a departure from the approach of Chinnery, our object will be to develop the formulae for the displacement field and stress changes which are representative of a dislocation surface showing variable vertical and constant horizontal slip. This allows us to examine a fault model which is perhaps more realistic.

This dissertation is divided into three main sections. The first (Chapter 2) contains the theoretical approach to the problem as well as the expressions which are necessary to calculate analytical solutions. The second part (Chapter 3) is primarily concerned with interpretations of the analytical results acquired. Finally, Chapters 4 and 5 deal directly with application of the theoretical results to various geological observations.

CHAPTER 1

HISTORICAL REVIEW

We will begin our discussion with a brief outline of the historical background of the subject. In particular, we shall mention the theoretical approaches of other authors and show how their work was severely limited by their initial assumptions.

1.1 The Concept of Fracture

The concept of dislocations (Love, 1944), originally referred to as distortions, was introduced into elasticity theory by Volterra in order to describe the deformation that may arise in a body occupying a multiply-connected region, when the displacements of its points are given by many-valued functions of the co-ordinates (in the absence of body forces). As a result, very small fractures have been examined by several authors. Inglis (1913), Sneddon (1946), and Griffith (1921, 1924) have focussed their attention on the microscopic causes of fracture. The nature of their work is very similar to ours, the main difference, being the magnitude of the fractures involved.

1.2 Application of Fracture to Geology

Anderson (1951) using the theories of Navier, Coulomb, and Mohr considered a two dimensional fault of finite length and infinite depth but took no account of the boundary condition at the ground surface. He adapted the elliptical crack of Inglis (1913) as a model for his strike-slip fracture only to find that few deductions could be inferred from his results.

Kasahara (1957, 1958, 1959) after postulating a continuous variation of displacement with depth, considered a fault of infinite length and finite depth. He then applied basic elasticity theory to calculate the disturbance of the surrounding medium. His results were plausible but could not be used to describe a fault of finite length, the case most prevalent in the earth's crust.

Byerly and De Noyer (1958) attempted to determine the depths of several actual fractures by calculating the shear strain energy in the earth just before faulting occurs. They assumed that the deformation of strain at the earth's surface remained unaltered to that depth at which the fault broke and no deeper. Although their depth estimates seemed very reasonable (in comparison with those determined using dislocation theory),

Byerly and De Noyer indicated that they were not convinced by the results.

Steketee (1957, 1958a) developed an "elasticity theory of dislocations" to investigate the changes brought about by the occurrence of faulting in nature. He applied a Green's function technique to the fundamentals of dislocation theory (Volterra, 1907), thus constructing a method for handling surfaces of discontinuity in an elastic solid. The advantage of this approach is not only that the condition of zero stress at the ground surface is inherent in the theory, but also, that it allows us to consider normal, reverse, and dipping faults as well as transcurrent strike-slip fractures.

Chinnery (1959, 1962) applied Steketee's "elasticity of dislocations" to a vertical rectangular strike-slip fault which may or may not intersect the ground surface. Various aspects of the displacement field and stress changes were included in his analyses of this constant slip model. Applications of his results to geodetic measurements were considered, especially as a means of determining the depths of various faults and the magnitudes of the stresses that caused the fractures to occur. Although Chinnery's model was only a mathematical approximation to a geological situation, it

produced several realistic results (Press, 1965). Hence, he proceeded to examine a strike-slip fault model that displays a variable horizontal slip and a constant vertical slip. His interpretations of the results have not yet been completed but they should be of considerable interest when compared with those outlined in this thesis.

1.3 Basic Assumptions of Dislocation Theory

It would be impossible to apply dislocation theory to obtain analytical results if a simple mathematical model were not used. It is usual in mathematical analyses to retain only those features which are believed to be of major importance. In our case this means that we shall concern ourselves with a semi-infinite homogeneous, isotropic medium where the laws of the classical theory of elasticity hold. Such features as the curvature of the earth, its gravitational and magnetic fields, temperature, and non-homogeneity will not be considered. It is also important to recall the assumptions that are implicit in the theory. The most important of these are that the earth's crust may be regarded as an elastic solid and that infinitesimal strain theory is applicable.

Furthermore, we shall restrict ourselves to static problems which implies that waves and other transient features associated with earthquakes will not be considered. This is a reasonable assumption since earthquake fractures occur within a matter of a few minutes (Scheidegger, 1957), and hence we expect elasticity theory to be applicable to the immediate effects of faulting. The process of fracture, of course, is basically non-elastic, but it has been shown (Chinnery, 1964) that faults appear under applied stresses of as much as two orders of magnitude less than the breaking strength of rock as measured in the laboratory. Under these circumstances, it is plausible that the laws of elasticity should apply even to the material in the immediate vicinity of the fault face.

CHAPTER 2

THE DISPLACEMENT FIELD AND STRESS CHANGES DUE TO A
RECTANGULAR DISLOCATION WITH VARIABLE SLIP

An outline of the theory leading up to the evaluation of the displacement field, the stress changes, and the maximum shear stress that result from the introduction of a variable-slip dislocation into a semi-infinite elastic medium are given below. All expressions are finally reduced to the case $\lambda = \mu$ and reference is made, where applicable, to their physical significance.

The notation used throughout this thesis follows that of Steketee (1957, 1958a, 1958b), Sokolnikoff (1956), and Chinnery (1962).

2.1 The Equations of Elasticity

If x_i ($i = 1, 2, 3$) is a Cartesian co-ordinate system and $u(x_i)$ the displacement field produced by a force system within a homogeneous isotropic elastic solid, then the components of the strain tensor e_{ij} and of the stress tensor τ_{ij} are given by the relations

$$e_{ij} = \frac{1}{2} (u_{i,j} + u_{j,i}) \quad (2.1)$$

$$\tau_{ij} = \lambda \delta_{ij} u_{k,k} + \mu (u_{i,j} + u_{j,i}) \quad (2.2)$$

where λ and μ are Lamé's constants, δ_{ij} the Kronecker symbol, and $u_{i,j} = \frac{\partial u_i}{\partial x_j}$. Equation (2.2) is commonly referred to as the generalized form of Hooke's Law (Sokolnikoff 1956). On substituting the equations of equilibrium (in the absence of body forces - equations 2.3)

$$\tau_{ij,j} = 0 \quad (2.3)$$

into equation (2.2) we obtain Navier's equations

$$\mu u_{i,jj} + (\lambda + \mu) u_{j,ji} = 0 \quad (2.4)$$

which play the same role in dislocation theory that Laplace's equations do in ordinary potential theory.

2.2 The Basic Equations

A dislocation surface Σ is defined as one across which there is a discontinuity in one or all of the components of the displacement vector u_i . Steketee (1958a) uses the Green's function method to deal with the problem of a Volterra dislocation in a

semi-infinite medium in such a way that the boundary surface of the medium remains stress free. A Volterra dislocation is here defined as a surface across which the displacement components show a discontinuity of the form

$$\Delta u_i = u_i + \Omega_{ij} x_j \quad (2.5)$$

$$\Omega_{ij} = -\Omega_{ji}$$

where u_i and Ω_{ij} are constants. The relation (2.5b), which is the well-known Weingarten relation (Weingarten, 1907), implies that the discontinuity across Σ is of the form of a rigid body displacement. In the following applications we shall assume that the rotation matrix Ω_{ij} is zero. This implies that there is no net rotation of the fault faces relative to one another during the process of fracture.

By solving this fairly complex boundary value problem which stipulates a condition of zero stress on the surface, Steketee (1958a) obtained the general solution for the displacement field u_k , in a semi-infinite medium due to the dislocation Δu_i , in the form

$$u_k = \frac{1}{8\pi\mu} \iint_{\Sigma} \Delta u_i w_{ij}^k v_j d\Sigma \quad (2.6)$$

Here ν_j represents the direction cosines of the normal to the surface element $d\Sigma$. The Green's functions ω_{ij}^k are the displacement fields in a semi-infinite medium due to a set of nuclei of strain defined by i and j (see Love 1944, p. 186); the superscript refers to the different fields. These nuclei of strain are elementary force systems with moment (for $i \neq j$) and without moment (for $i = j$). A total of six functions ω_{ij}^k (for $i = 1, 2, 3$; $j = 1, 2, 3$; $ij = ji$) are needed for the solution of the general surface Σ .

The problem in which we are interested requires a nucleus that has two double forces in the plane parallel to the boundary. Using $X_3 = 0$ as the surface of the medium Steketee has evaluated the function ω_{12}^k which satisfies these requirements. This allows us to integrate over the plane surface $y_2 = 0$ with a variable discontinuity in the x_1 component of the displacement vector. Physically, this means that we can determine the displacements produced throughout the medium by a vertical strike-slip fault.

2.3 Galerkin Vectors

Since several of the expressions with which we must deal may become extremely clumsy, we shall

make use of Galerkin vectors (Galerkin 1930; Papcovitch 1932). Although these vectors do not help much in the actual solution of the problem, they enable us to state the results as compactly as possible.

The Galerkin vector Γ_i is defined as a vector which gives a displacement field by differentiating according to the Laplace operator and grad div. Therefore, if the Galerkin vector for a problem is known, the problem is solved, as the displacements are given by the expression

$$u_k = \Gamma_{k,ii} - \alpha \Gamma_{i,ik} \quad (2.7)$$

where

$$\alpha = \frac{\lambda + \mu}{\lambda + 2\mu}$$

Hence, we have immediately for the strains e_{ij} and the stresses τ_{ij} ,

$$\begin{aligned} e_{ij} &= \frac{1}{2} (\Gamma_{i,jkk} + \Gamma_{j,ikk}) - \alpha \Gamma_{k,kij} \\ \tau_{ij} &= \lambda(1-\alpha) \delta_{ij} \Gamma_{k,kll} + \mu (\Gamma_{i,jkk} + \Gamma_{j,ikk}) \\ &\quad - 2\mu \alpha \Gamma_{k,kij} \end{aligned} \quad (2.8)$$

The substitution of u_i into the Navier equations (2.4) now leaves us with the equation

$$\text{or } \Gamma_{i,jjkk} = 0 \quad (2.9)$$

$$\nabla^4 \Gamma_i = 0$$

which shows that each component of the Galerkin vector is biharmonic. This is a definite advantage since the general solution to such an equation has a form which is much simpler than the corresponding solution of Navier's equations.

2.4 The Galerkin Vectors for the Displacement Field

Steketee quotes the Green's function ω_{12}^k in terms of a Galerkin vector Γ_{12}^k (Westergaard, 1952). In this case equation (2.6) becomes

$$\Gamma_k = \frac{1}{8\pi\mu} \iint_{\Sigma} u_i \Gamma_{12}^k d\Sigma \quad (2.10)$$

where Γ_{12}^k is the Galerkin vector for the displacement field at an observation point (y_1, y_2, y_3) due to a nucleus at the point $(x_1, 0, x_3)$ on the dislocation surface. The components of this Galerkin vector were given by Steketee and generalized by Chinnery as follows:

$$\Gamma_{12}^1 = -\mu y_2 \left(\frac{1}{s_1} + \frac{1}{s_2} \right)$$

$$\Gamma_{12}^2 = \mu t \left(\frac{1}{s_1} + \frac{1}{s_2} \right)$$

$$\Gamma_{12}^3 = \frac{\mu t y_2}{(s_2 + p)^2} \left[2c - 2 \frac{(bp+q)}{s_2} - \frac{(p^2 - q^2)(2s_2 + p)}{s_2^3} \right]$$

(2.11)

where: $p = x_3 + y_3$

$$q = x_3 - y_3$$

$$t = x_1 - y_1$$

$$s_1^2 = t^2 + y_2^2 + q^2$$

$$s_2^2 = t^2 + y_2^2 + p^2$$

$$b = \frac{\lambda - \mu}{\lambda + \mu}$$

$$c = \frac{\mu \lambda}{(\lambda + \mu)^2}$$

A consideration of equation (2.10) indicates that we can now calculate the displacement field due to a vertical transcurrent fault model whose dislocation is over a plane surface containing the y_3 axis and perpendicular to either the y_1 or y_2 axes (figure 2.1). This implies that the discontinuity u_k must be in the y_2 or y_1 direction respectively.

2.5 Integration over the Dislocation Surface

At this stage in the analysis, in order to simplify all future work we make the assumption that $\lambda = \mu$, which is not unusual in the application of elasticity theory to geophysics. It follows that $\alpha = 2/3$, $b = 0$, and $c = 1/4$.

The orientation and dimensions of the dislocation surface Σ , over which we are to integrate are shown in figure 2.1. We assume that the discontinuity u_k in displacement at the fault

face has only one component u_1 which is a function of the vertical position x_3 alone i.e. the fault is an entirely transcurrent, variable-slip dislocation. If we represent this discontinuity by $u_1(x_3)$ then $u = u_1(0)$ will be the total relative displacement of the two sides of the fault on the ground surface.

The introduction of these modifications into equations (2.7) and (2.10) requires that we evaluate the displacement field u_k given by

$$u_k = \Gamma_{k,ii} - \frac{2}{3} \Gamma_{i,ik} \quad (2.12)$$

$$\Gamma_k = \frac{1}{8\pi\mu} \int_{-L}^L \int_D \Gamma_{12}^k u_1(x_3) dx_1 dx_3$$

The evaluation of equation (2.12b) and its subsequent substitution into equation (2.12a) to obtain the displacements is very long and tedious. As a result, only an outline of the procedure followed will be given here. Further details are given in appendix A.

First we introduce the expressions ϵ_k and ω_k which are defined respectively by the equations

$$\epsilon_k = \int_{-L}^L \Gamma_{12}^k dx_1 \quad (2.13)$$

$$\omega_k = \epsilon_{k,ii} - \frac{2}{3} \epsilon_{i,ik}$$

Such a representation is possible only because the observation point does not lie on the dislocation surface. This allows one to perform differentiations with respect to y_i inside the integral without distorting the original problem.

For the sake of brevity we shall use the sign \parallel after an equation to represent the substitution $f(x_1, x_3) \parallel = f(L, x_3) - f(-L, x_3)$. The components of the term ω_k are then found to be:

$$\begin{aligned}\omega_1 &= -2\mu y_2 (F_1 + \frac{t}{3} F_2) \parallel \\ \omega_2 &= \frac{2}{3}\mu (F_3 + y_2^2 F_2) \parallel \\ \omega_3 &= \frac{2}{3}\mu y_2 F_4 \parallel\end{aligned}\tag{2.14}$$

where

$$F_1 = \frac{1}{s_2(s_2+t)} + \frac{1}{s_1(s_1+t)}$$

$$F_2 = \frac{1}{s_2^3} + \frac{2}{s_1^3} + \frac{3p(2s_2+p)}{s_2^3(s_2+p)^2} - \frac{12x_3y_3}{s_2^5}$$

$$F_3 = \frac{2}{s_2+p} + \frac{1}{s_1} - \frac{p}{s_2(s_2+p)} + \frac{4x_3y_3}{s_2^3}$$

$$F_4 = \frac{3}{s_2(s_2+p)} + \frac{2(y_3-3x_3)}{s_2^3} - \frac{12x_3y_3p}{s_2^5} - \frac{2q}{s_1^3} + \frac{2p}{s_2^3}$$

and

$$p = x_3 + y_3$$

$$q = x_3 - y_3$$

$$t = x_1 - y_1$$

$$s_1^2 = t^2 + y_2^2 + q^2$$

$$s_2^2 = t^2 + y_2^2 + p^2$$

Hence the components of the displacement vector are found from the equation

$$u_k = \frac{1}{8\pi\mu} \int_D^D u_i(x_3) \omega_k dx_3 \quad (2.15)$$

Because of the complexity of the integrand in equations (2.15) it is necessary to employ numerical methods to obtain solutions to the integral. This will be discussed in greater detail in the following chapter.

2.6 Expressions for the Stress Change

Steketee (1957) has shown that the stress changes that result from the introduction of a dislocation into an elastic medium are independent of any stress distribution that existed beforehand. In this section we are concerned only with the stress changes produced in a semi-infinite elastic medium by a variable

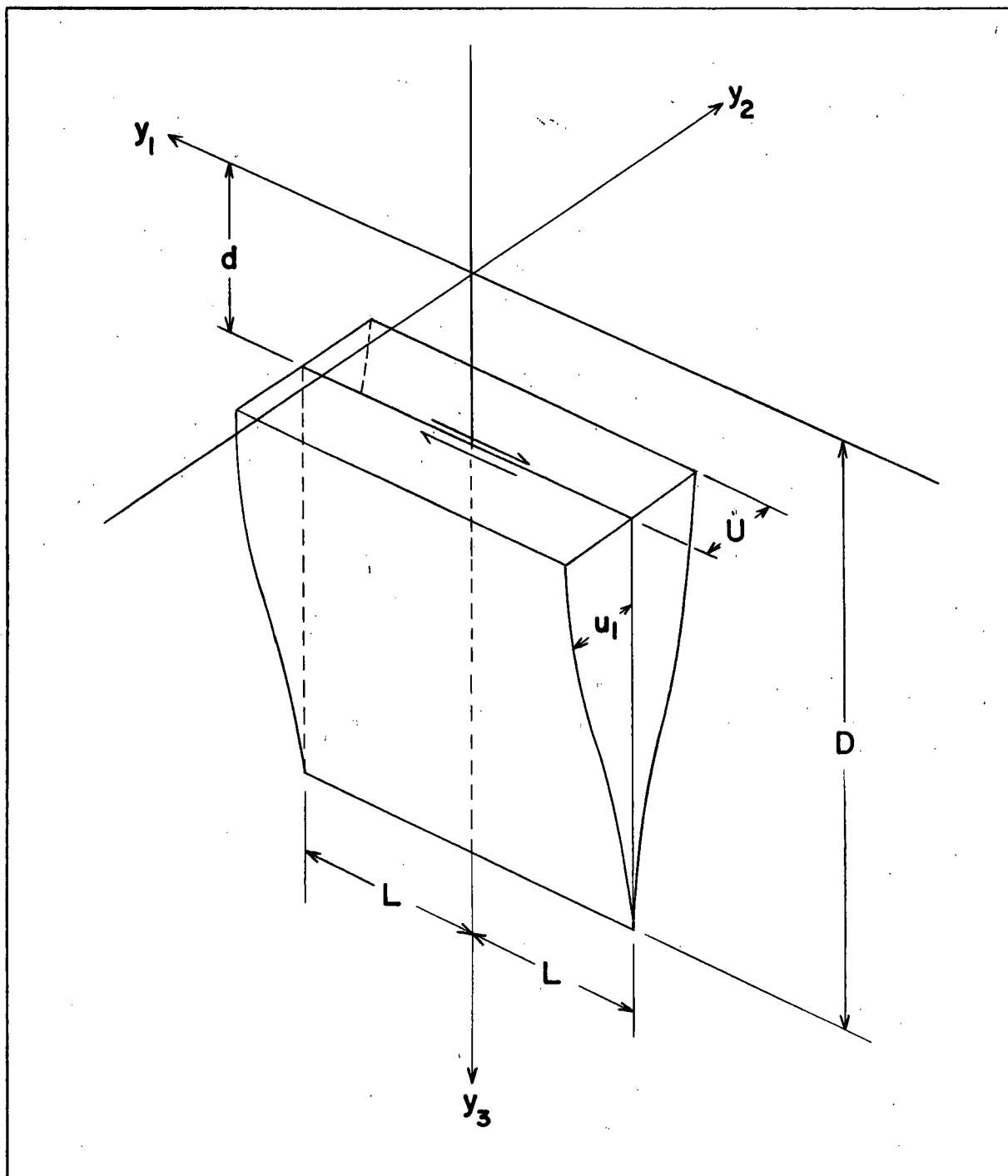


Figure 2.1.

Dimensions of the Variable-Slip Model

Rectangular Dislocation

($y_3 = 0$ represents the ground surface)

slip dislocation as shown in figure 2.1.

We differentiate the Galerkin vector Γ_{12}^k to obtain the displacement components u_k ,

$$u_k = \Gamma_{k,ii} - \frac{2}{3} \Gamma_{i,ik}$$

We may now obtain the stress changes associated with this displacement field by differentiating u_k according to Hooke's Law (equation 2.8b). As in the previous section we differentiate with respect to y_i inside the integral and use the notation \parallel to denote $f(x_1, x_3) \parallel = f(L, x_3) - f(-L, x_3)$.

The differentiation of equations (2.14) is algebraically very complex. As a result, we will quote here only the nine derivatives $\omega_{i,j}$. Further details are given in appendix B.

$$\begin{aligned} \omega_{1,1} &= -\frac{2}{3} \mu y_2 (3G_1 - F_2 + t^2 G_2) \parallel \\ \omega_{1,2} &= -2\mu (F_1 - y_2^2 G_3) - \frac{2}{3} \mu t (F_2 - y_2^2 G_2) \parallel \\ \omega_{1,3} &= 2\mu y_2 G_4 - \frac{2}{3} \mu y_2 t G_5 \parallel \\ \omega_{2,1} &= \frac{2}{3} \mu t G_6 + \frac{2}{3} \mu t y_2^2 G_2 \parallel \\ \omega_{2,2} &= -\frac{2}{3} \mu y_2 (G_6 + y_2^2 G_2) \parallel \\ \omega_{2,3} &= \frac{2}{3} \mu (G_7 + y_2^2 G_5) \parallel \end{aligned} \tag{2.16}$$

$$\omega_{3,1} = \frac{2}{3} \mu y_2 t G_8 \parallel$$

$$\omega_{3,2} = \frac{2}{3} \mu (F_4 - y_2^2 G_8) \parallel$$

$$\omega_{3,3} = \frac{2}{3} \mu y_2 G_9 \parallel$$

where:

$$F_1 = \frac{1}{s_2(s_2+t)} + \frac{1}{s_1(s_1+t)}$$

$$F_2 = \frac{1}{s_2^3} + \frac{2}{s_1^3} + \frac{3p(2s_2+p)}{s_2^3(s_2+p)^2} - \frac{12x_3y_3}{s_2^5}j_3$$

$$F_4 = \frac{3}{s_2(s_2+p)} + \frac{2(y_3-3x_3)}{s_2^3} - \frac{12x_3y_3p}{s_2^5}j_3 - \frac{2q}{s_1^3} + \frac{2p}{s_2^3}$$

$$G_1 = \frac{3}{s_2^3} + \frac{3}{s_1^3}$$

$$G_2 = \frac{3}{s_2^5} + \frac{6}{s_1^5} + \frac{3p(8s_2^2+9ps_2+3p^2)}{s_2^5(s_2+p)^3} - \frac{60x_3y_3}{s_2^7}j_3$$

$$G_3 = \frac{2s_2+t}{s_2^3(s_2+t)^2} + \frac{2s_1+t}{s_1^3(s_1+t)^2}$$

$$G_4 = \frac{p(2s_2+t)}{s_2^3(s_2+t)^2} - \frac{q(2s_1+t)}{s_1^3(s_1+t)^2}$$

$$G_5 = \frac{-3p}{s_2^5} + \frac{6q}{s_1^5} + \frac{3(2s_2+p)}{s_2^3(s_2+p)^2} - \frac{3(3p+4x_3)}{s_2^5} + \frac{60x_3y_3p}{s_2^7}$$

$$G_6 = \frac{2}{S_2(S_2+p)^2} + \frac{1}{S_1^3} - \frac{p(2S_2+p)}{S_2^3(S_2+p)^2} + \frac{12x_3y_3}{S_2^5}$$

$$G_7 = \frac{q}{S_1^3} - \frac{3}{S_2(S_2+p)} + \frac{p+4x_3}{S_2^3} - \frac{12px_3y_3}{S_2^5}$$

$$G_8 = \frac{3(2S_2+p)}{S_2^3(S_2+p)^2} + \frac{6(p-4x_3)}{S_2^5} - \frac{60x_3y_3p}{S_2^7} - \frac{6q}{S_1^5} + \frac{6p}{S_2^5}$$

$$G_9 = -\frac{1}{S_2^3} + \frac{6pq}{S_2^5} + \frac{12x_3y_3(5p^2-S_2^2)}{S_2^7} - \frac{2(3q^2-S_1^2)}{S_1^5} - \frac{2(3p^2-S_2^2)}{S_2^5}$$

and

$$p = x_3 + y_3$$

$$q = x_3 - y_3$$

$$t = x_1 - y_1$$

$$S_1^2 = t^2 + y_2^2 + q^2$$

$$S_2^2 = t^2 + y_2^2 + p^2$$

We now express Hooke's Law (equation 2.2) in terms of the derivatives $\omega_{i,j}$ to obtain the general expression

$$\tau_{ij} = \frac{1}{8\pi} \int_D u_1(x_3) (\delta_{ij} \omega_{k,k} + \omega_{i,j} + \omega_{j,i}) dx_3 \quad (2.17)$$

where $u_1(x_3)$ represents the discontinuity in displacement as defined in section (2.5) and $\lambda = \mu$. The tensor is, of course, symmetric ($\tau_{ji} = \tau_{ij}$) and must satisfy the following boundary conditions at the surface of the medium ($y_3=0$):

$$\tau_{13} = \tau_{23} = \tau_{33} = 0 \quad (2.18)$$

We can show that equations (2.17) satisfy these conditions and as a result will assume that no algebraic errors exist in them.

At this point it is necessary to evaluate the integrals (2.17). Although the expressions are algebraically long, they can be evaluated with little difficulty, and in as much accuracy as possible with the aid of an electronic computer (the present calculations were performed on the I.B.M. 7040 computer).

2.7 The Maximum Shear Stress

It is well known that a set of three homogeneous equations in unknown directions \vec{v} such as

$$(\tau_{ij} - \tau \delta_{ij}) v_j = 0 \quad (2.19)$$

has a non-trivial solution if, and only if, the determinants of the coefficients of the v_j is equal to

zero

$$\text{i.e. } |\tau_{ij} - \tau \delta_{ij}| = 0 \quad (2.20)$$

This cubic equation in the stress τ has three real roots τ_1, τ_2, τ_3 , called the principal stresses. Knowing these roots, the corresponding principal directions of stress τ_{ij} can be determined. In other words, the magnitudes and directions of the principal stresses are simply the eigenvalues and eigenvectors, respectively, of the matrix τ_{ij} .

Given the magnitudes and directions of the principal stresses at any point, the corresponding values of the maximum shearing stress are easily determined. The magnitude of this shear stress is numerically equal to one-half the difference between the greatest and least principal stresses (assume $\tau_3 > \tau_2 > \tau_1$) and acts on the plane that bisects the angle between the directions of the largest and smallest principal stresses,

$$\text{i.e. } |\tau_{\max}| = \frac{\tau_3 - \tau_1}{2} \quad (2.21)$$

Since there is no satisfactory way to represent a three dimensional stress distribution (equation

2.7) diagrammatically without omitting much of the information contained in the full equations, the maximum shear stress is physically the most meaningful quantity for discussing shear fractures. Furthermore, it is worth noting that if an initial stress distribution (τ_{12}° in our case) is superimposed on the calculated stress change τ_{ij} (this is what actually happens in a physical situation), the principal axes of stress and hence the planes of maximum shear stress will assume a completely different form which is of no immediate use to us here. For this reason, in the following discussion we will be concerned only with the magnitude of the maximum shear stress and not with its direction. Appendix C contains more detailed information regarding the maximum shear stress.

CHAPTER 3

COMPUTATION OF THE DISPLACEMENTS AND STRESS CHANGES
PRODUCED BY VARIOUS FAULT MODELS

In order to provide a physical background for the ideas of dislocation theory that have been developed, we consider here various fault models which are able to account for observations made on actual earthquakes. In particular, we are interested in a fault model which exhibits a constant slip in the horizontal direction and a variable slip in the vertical plane.

Discussions of various aspects of this problem may be found in Kasahara (1958a, 1958b), Steketee (1958b), Byerly and De Noyer (1958) and Chinnery (1959, 1962, 1964).

3.1 The Basic Model

Anderson (1951) defines the standard state in the earth as that of a hydrostatic pressure. Thus it represents a condition in which the lateral pressure from all sides increases steadily with depth so as to be equal everywhere to the vertical pressure. The

latter is determined approximately by the weight of the overlying rock and is roughly proportional to depth provided that there are no great variations in density. Such variations would arise only when the strata above the point under consideration are functioning as an arc as, for example, in the centre of an anticline. Therefore, in most cases it is reasonable to assume that the discontinuity u_1 will die out towards the bottom of the fault.

If the coefficient of friction is constant (which is not known) then $u_1(x_3)$ should decrease linearly with depth. However, it has been shown (Chinnery, 1962) that accumulations of stress around the lower edge of the fault may cause it to extend somewhat deeper. Thus it is plausible to assume that there is a functional variation of $u_1(x_3)$ with depth.

The available energy represented by the condition of stress in the earth's crust must overcome not only the strength of the material but also the internal friction opposing the motion, if fracture is to occur. This frictional resistance along the fault plane is proportional to the normal pressure across the fault faces (the τ_{22} component of the stress change in this case). As a result, it will have a tendency,

not only to reduce the magnitude of the slip u_1 , in depth (τ_{22} increases with depth), but also to contribute to the production of heat along the interface. The latter condition may be associated with the plastic effects observed close to the dislocation surface.

Although we have no knowledge of the discontinuity over the face of a real fault, the geodetic conditions outlined in the previous three paragraphs gives some justification for the use of a fault model which exhibits a variable slip $u_1(x_3)$ in the vertical plane. A constant slip $u_1(x_1) = U$ in the horizontal plane is also a necessary assumption. For, if $u_1(x_1)$ is allowed to vary from point to point, the computer time required to produce convergent solutions to the double numerical integrations (2.10) would be prohibitive.

The aforementioned considerations have encouraged us to choose a variable-slip model whose dislocation surface is described by the function

$$u_1(x_3) = U \exp \left[-a \left(\frac{x_3 - b}{c} \right)^2 \right] \quad (3.1)$$

where a, b, c are constants which may be varied

until the desired discontinuity is obtained and is the maximum value of the slip. This model, however, does not allow the slip u_1 to diminish towards the ends of the fault as we would intuitively expect; instead, mathematical singularities arise in these regions. Fortunately, the latter are of little consequence as long as we do not carry out an analytical analysis in this critical area.

3.2 Evaluation of the Integrals Using Numerical Procedures

The task of evaluating equations (2.15) and (2.17) which represent the displacement field and stress changes respectively, would be prohibitive without the aid of an electronic computer. Hence, these equations were evaluated on the I.B.M. 7040 at the University of British Columbia.

Two quadrature formulae were applied to equations (2.15) and (2.17) in order to obtain analytical expressions for the displacement field and the stress changes. The first of these, Simpson's Rule (see Nielsen, 1957), was easily adaptable to our equations but did not produce accurate results unless the range of integration was very finely divided. This meant that considerable computer time was required to obtain

only reasonably accurate answers. As a result, we used the Gaussian quadrature (see Nielsen, 1957) throughout our analyses. Such an approach requires that the integration procedure be entirely dependent on the zeros of the Legendre polynomials and their respective weighting functions. The integrals were evaluated both accurately and efficiently using this method.

In most regions around the dislocation surface the numerical evaluation of the integrals was carried out without any trouble. This included both the area near the ground surface and that region around the bottom of the fault; in both cases the fall-off of the integrands were everywhere continuous. However, analytical expressions could not be obtained for points very close to the fault face. In such areas the I.B.M. 7040 computer indicated that the calculations involved exceeded the machine's capacity, thus producing an overflow condition. This implies that the region extremely close to the surface of discontinuity, is represented by equations containing terms of the form $\frac{1}{x_i - y_i}$, where x_i and y_i are very nearly equal.

3.3 Computation of the Displacements and Stresses

We have programmed the I.B.M. 7040 computer at the University of British Columbia to evaluate the relevant analytical expressions.

All the necessary programmes were constructed in such a manner that:

- (a) d , D and L are input parameters and thus can be varied at any time,
- (b) calculations may be executed at any point in the y_i co-ordinate space by controlling data input,
- (c) the value of the slip u_1 may be specified as a relative or an explicit input parameter,
- (d) the computer output contains all the information pertaining to a given fault model.

Because equations (2.15) and (2.17) are symmetrical about the plane $y_1 = 0$ they were computed only for positive values of y_1 , y_2 and y_3 . Two basic approaches were used. The first enabled us to calculate the displacement field and the stress changes on the ground surface for various co-ordinates $(y_1, y_2, y_3) = (0, y_2, 0)$; the second, to generate a grid of any desired density in any plane $y_1 = k$ provided

that $|2K| < L$, the semilength of the fault (K is a constant). Hence, these analyses allow us to observe the fall-off of stress or displacement on the ground surface along $y_1 = 0$ and to examine contours of the same quantities in any vertical plane normal to the fault trace. Both of these aspects are illustrated later in this chapter as well as in chapters 4 and 5.

Four main programmes were set up. These were:

- (a) parallel displacement, u_1 ,
- (b) perpendicular displacement, u_2 ,
- (c) vertical displacement, u_3 ,
- (d) maximum shear stress, S_{max} .

The last case is applicable to any general situation. Its output includes analytical expressions for $\tau_{22}, \tau_{12}, \tau_{13}, \tau_{23}, \tau_{11}$, and τ_{33} as well as the coefficients and roots of the cubic equation obtained by diagonalizing the stress matrix (see appendix C).

3.4 Plotting of the Displacements

In order to compare the evaluations of equations (2.15) with geodetic observations made in the vicinity of surface faults, the constant d has been set equal to zero. Also, since a variable-slip model

will be used to approximate the depths of various faults two new terms will be defined. The first is the "effective depth" of a fault which will be used to describe that depth at which the slip u_1 falls to $\frac{1}{e}$ of its maximum value. The second is the "total depth" of a fault which will refer to that depth at which the slip u_1 has been reduced to about 2.5% of its maximum value. Where applicable, these values will be marked "E" and "T", respectively, on all of the graphs in this thesis.

Contour maps of the horizontal displacement, u_1 , were plotted for three basic models. Significant profiles were drawn to show the variation in properties exhibited by these. In all of them the displacements are expressed as percentages of the maximum slip $\frac{U}{2}$.

3.5 Horizontal Displacements

Contour maps of the horizontal displacements, u_1 , parallel to the fault are shown in figures 3.1 to 3.4. The first of these (3.1) was plotted by Chinnery (1961) who used a constant slip model as indicated on the plot. In the four cases presented little variation exists in the shape of the contours; rather, the main difference is in the rate of fall-off of the displace-

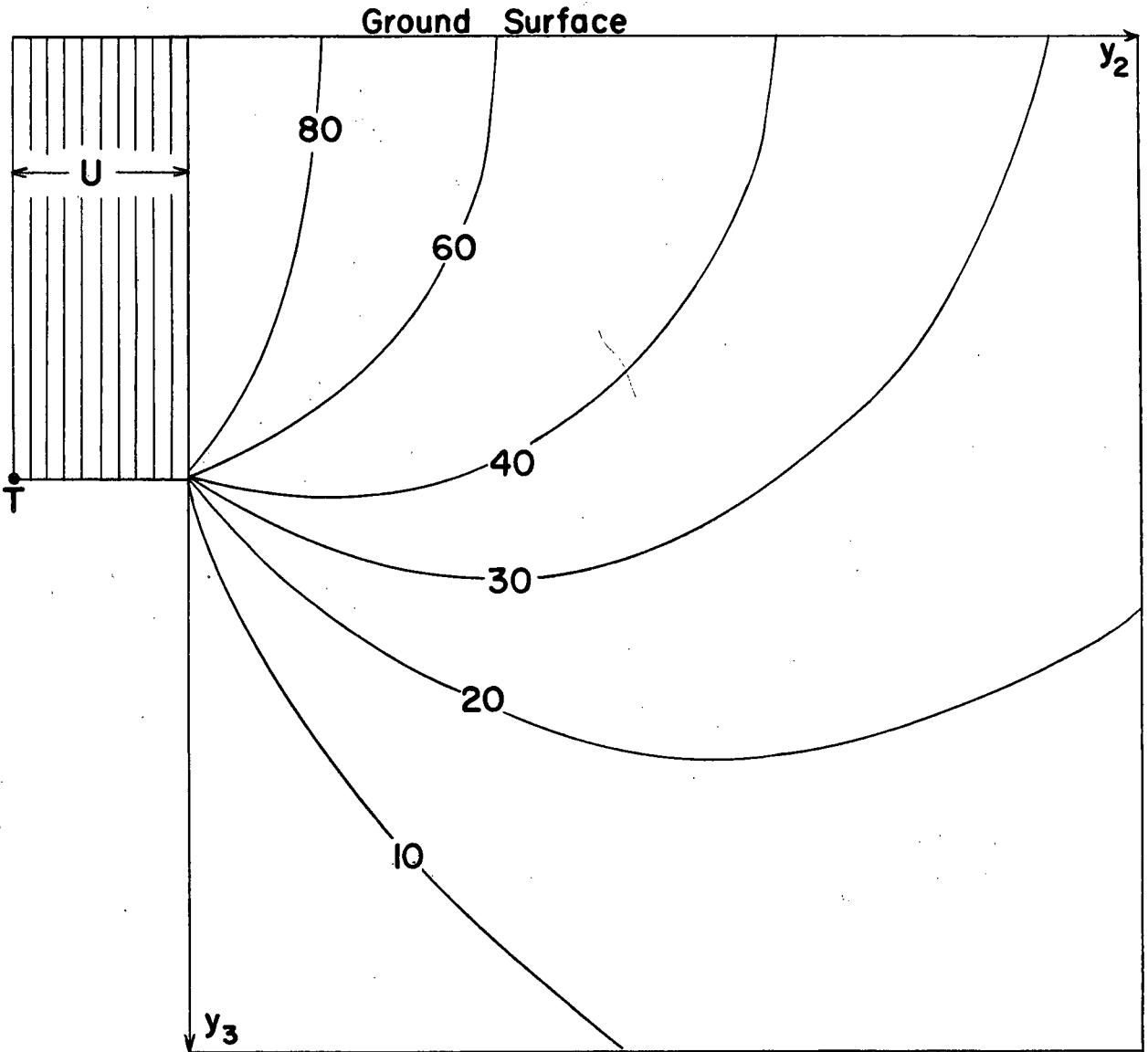


Figure 3.1

The horizontal displacement u_1 as a function of y_2 and y_3 in the vertical plane that bisects the fault at right angles. All contours are expressed as percentages of the maximum displacement $\frac{u}{2}$.

Chinnery 1961

$$y_1 = 0$$

$$u_1 = U$$

$$d = 0$$

$$L = 100$$

$$E = T = 0.1L$$

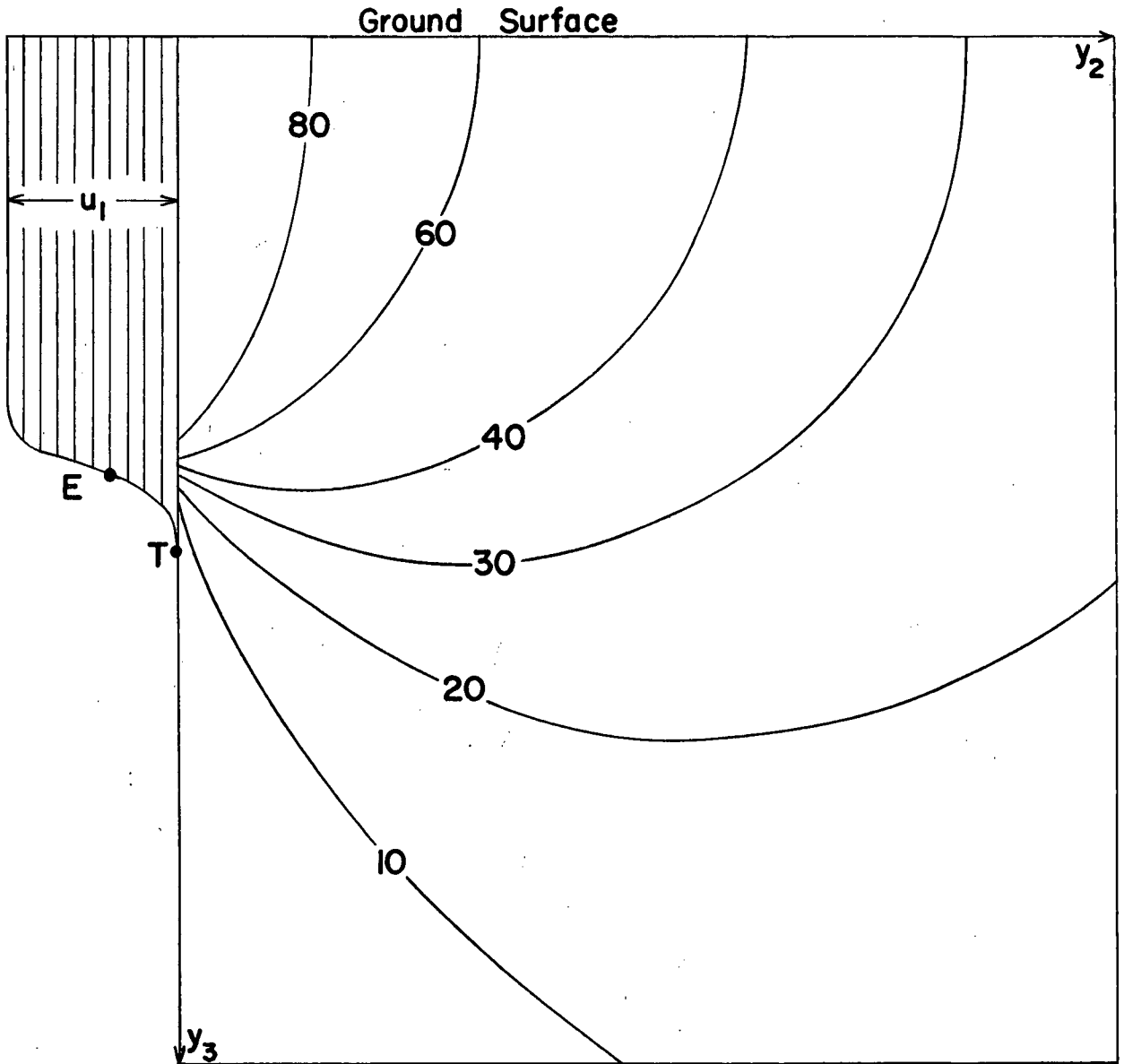


Figure 3.2

The horizontal displacement u_1 as a function of y_2 and y_3 in the vertical plane that bisects the fault at right angles. All contours are expressed as percentages of the maximum displacement $\frac{U}{2}$.

Model A

$$u_1 = U \exp \left[- \left(\frac{x_3 - 9}{3} \right)^2 \right]$$

$L = 100$

$y_1 = 0$

$d = 0$

$E = 0.1L$

$T = 0.12L$

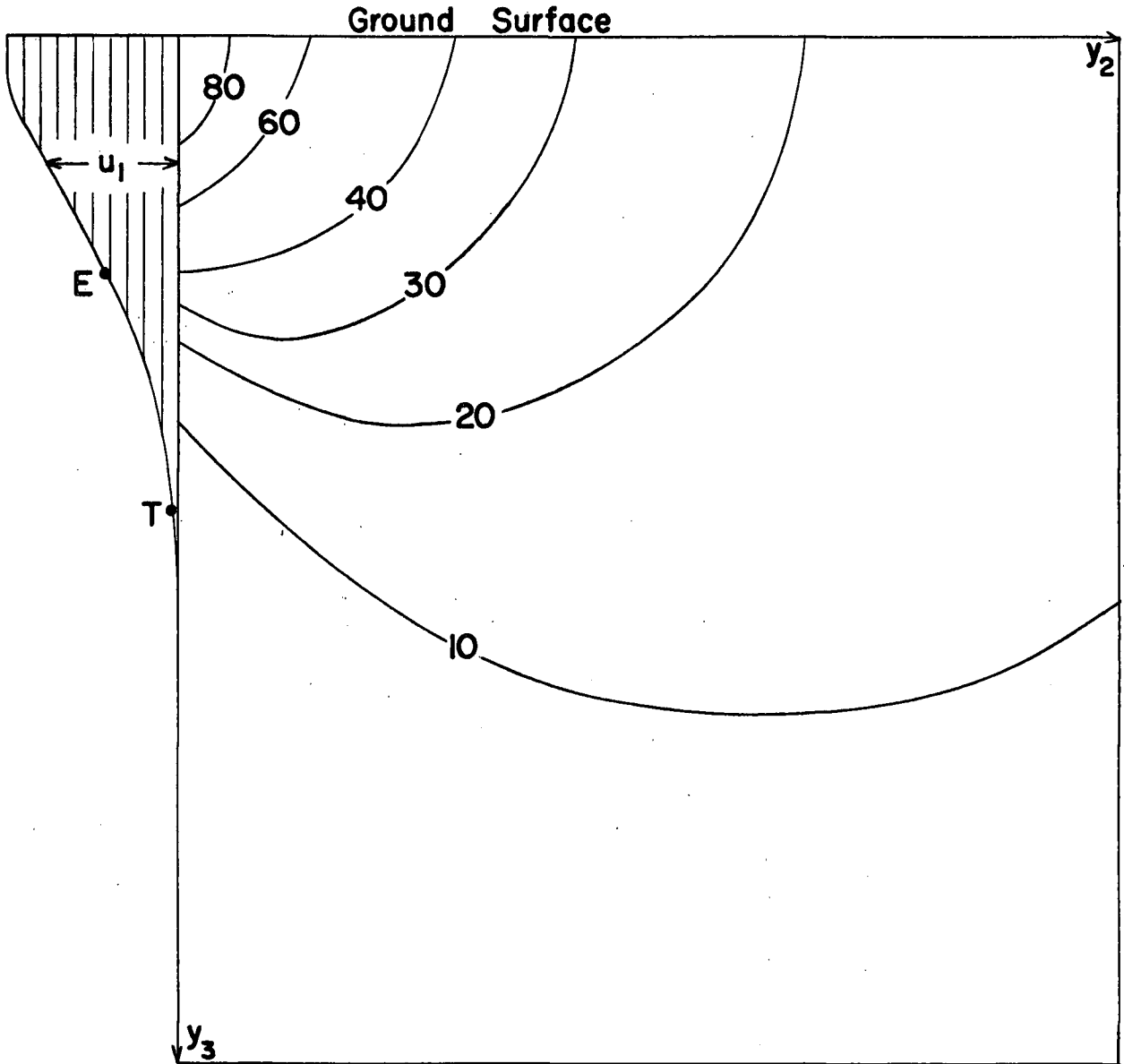


Figure 3.3

The horizontal displacement u_1 as a function of y_2 and y_3 in the vertical plane that bisects the fault at right angles. All contours are expressed as percentages of the maximum displacement $\frac{U}{2}$.

Model B

$$u_1 = U \exp \left[-0.5 \left(\frac{x_3}{4} \right)^2 \right]$$

$L = 100$

$y_1 = 0$

$d = 0$

$E = 0.06L$

$T = 0.11L$

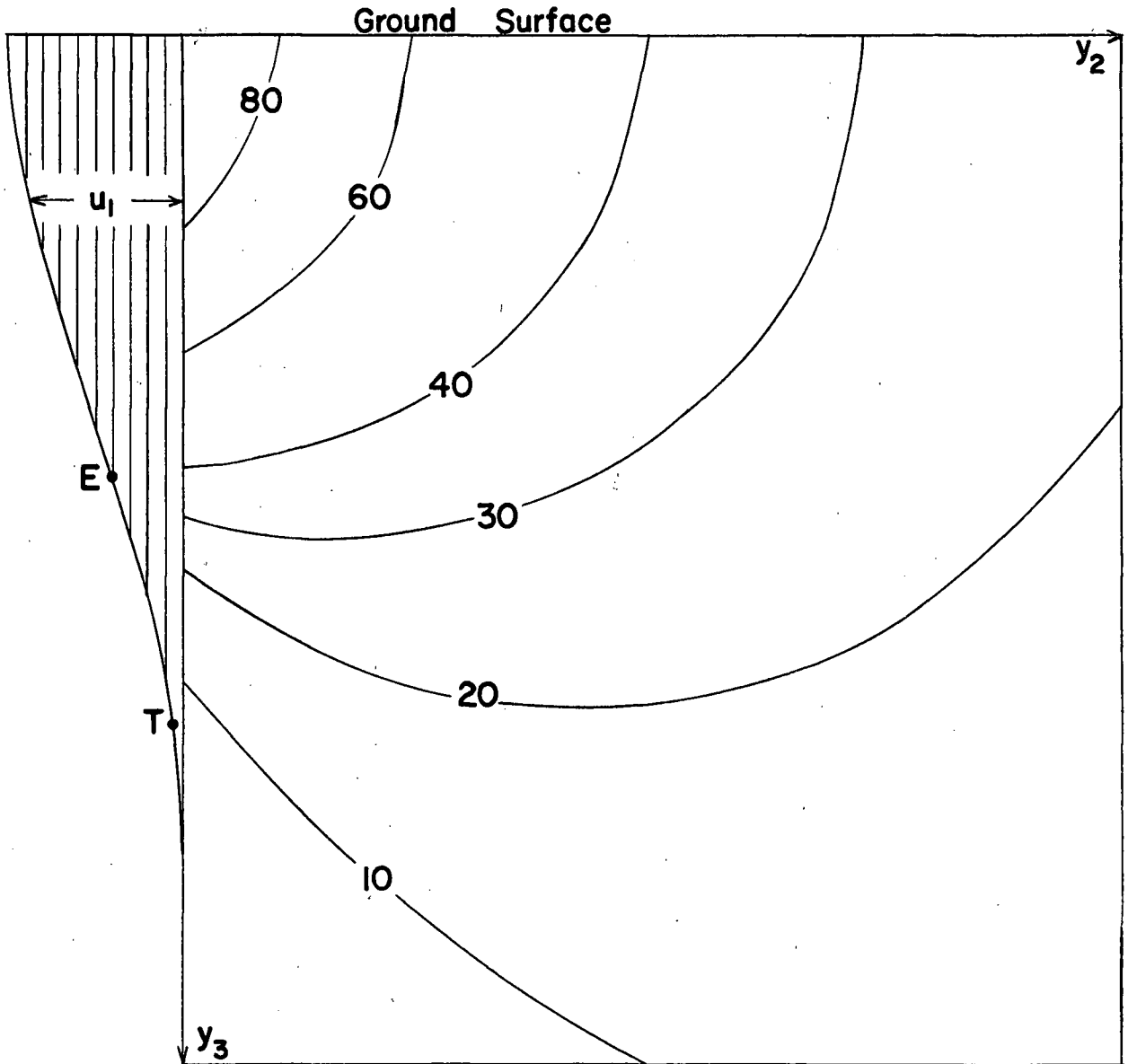


Figure 3.4

The horizontal displacement u_1 as a function of y_2 and y_3 in the vertical plane that bisects the fault at right angles. All contours are expressed as percentages of the maximum displacement $\frac{U}{2}$.

Model C

$$u_1 = U \exp \left[-0.2 \left(\frac{x_3}{4.5} \right)^2 \right]$$

$L = 100$

$$y_1 = 0$$

$$d = 0$$

$$E = 0.1L$$

$$T = 0.16L$$

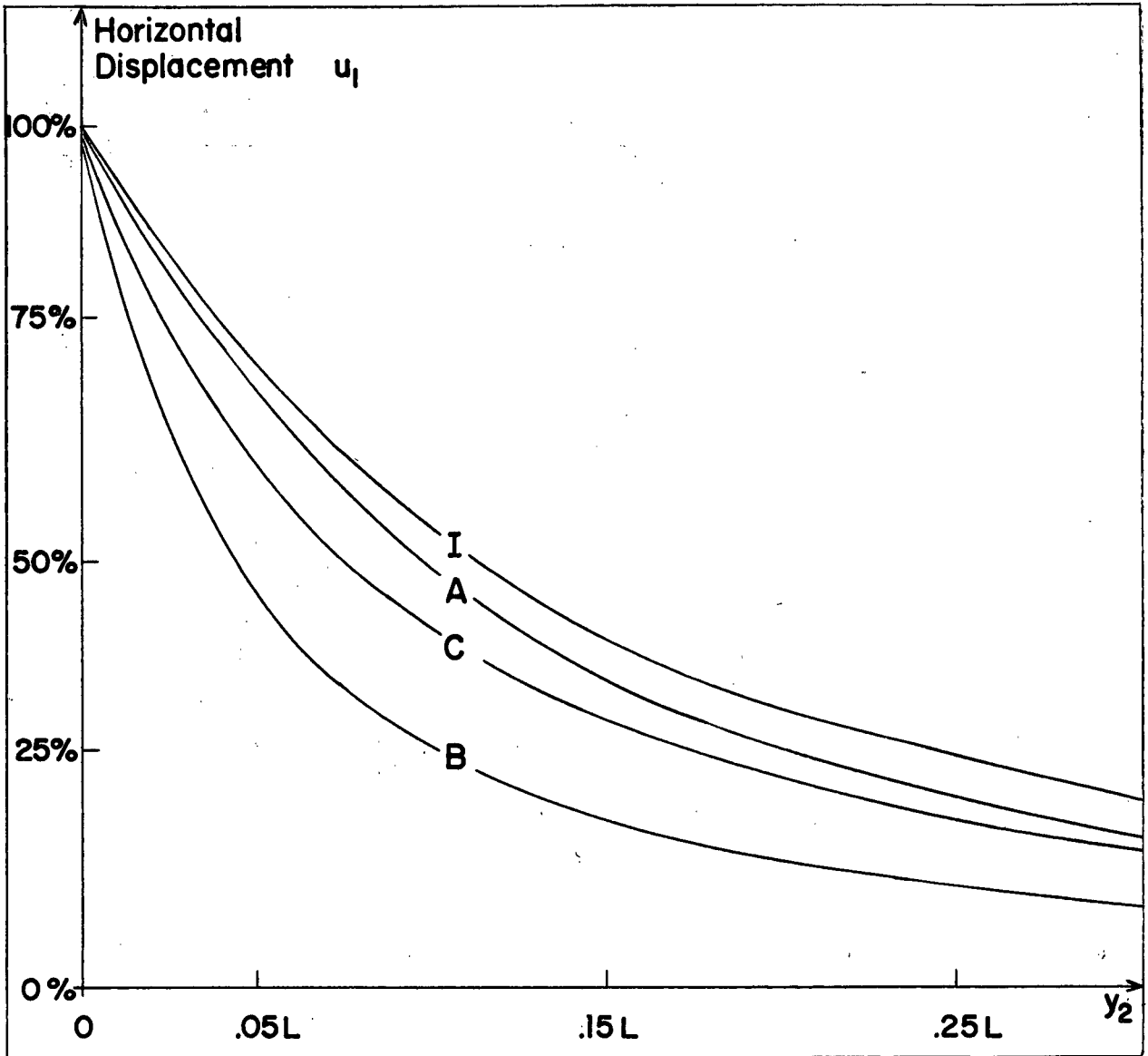


Figure 3.5

Fall-off of the horizontal displacement u_1 at the ground surface along a line that bisects the fault at right angles ($y_1 = 0$).

I Chinnery 1961

A Model A

B Model B

C Model C

ments with distance from the fault.

Figure 3.5 shows the fall-off of the displacement u_1 with y_2 along $y_1 = y_3 = 0$ for each of the above models. Profiles of this kind may be used to estimate the depths of actual faults (Chinnery, 1959). We use such an analysis in chapter 4 to approximate the depths of five fracture zones. The results of the survey are tabulated in table 4.1 so that they may readily be compared with the estimates of other authors.

3.6 Perpendicular Displacements

The perpendicular displacements, u_2 are of little interest to us in this thesis. However, evaluations of this displacement component were carried out at large distances from the dislocation surface (about $(y_1, y_2, y_3) = (3L, 3L, 0)$) so that a comparison could be made with values of the u_1 component. The analytical results for each of these components were nearly identical. This is to be expected at large distances from the fault model where each of the field components u_1 and u_2 should "see" the dislocation surface as a single nucleus. As a result, the calculated results lead us to believe that the mathematics

to this point in the analysis is correct. However, such a check of the equations is the only useful purpose of the u_2 evaluation.

3.7 Vertical Displacements

The vertical displacements u_3 , were evaluated for each of the fault models exhibited in figures 3.2 - 3.4. However, the results were so similar, (including the change of sign that occurs) to those of Chinnery (1961, 1965) that no further mention of the u_3 displacement components will be made at this point.

3.8 Plotting of the Stress Changes and Maximum Shear Stress

Once again only surface faults were considered and analyses were confined to the plane $y_1 = 0$.

Contour maps of the stress changes τ_{12} and τ_{13} were plotted in the plane $y_1 = 0$ for three basic models. These are illustrated in figures 3.6 to 3.11. Figure 3.12 demonstrates the fall-off of the stress change τ_{12} along y_2 ($y_1 = y_3 = 0$) for the above models. Calculations could not be made close to the dislocation surface (cf. Chapter 3.2).

Hence, the curves of figure 3.12 were extrapolated back (the dotted sections) to the fault plane

to enable us to obtain approximate values of the stress release at the origin, τ_{12}° (Chinnery, 1964). This term must be combined with the stress change τ_{12} in order that the principal stresses and hence the maximum shear stress can be calculated. τ_{12}° is assumed to be the initial stress component that causes fracture to occur.

Contour maps of the maximum shear stress were then plotted in the plane $y_1 = 0$ for each of the aforementioned models (figures 3.13 to 3.15). This analysis is applied to a specific fracture zone in chapter 5 in an attempt to relate the occurrence of aftershocks to transcurrent strike-slip faulting. Also, the values obtained for the stress release at the origin for each of the five faults discussed in chapter 4 have been entered in table 4.1 for the sake of completeness.

3.9 Results of the Horizontal Displacement Analyses

A careful examination of figures 3.1 to 3.5 indicates three definite trends. First of all the shapes of the contours of each of the four models analyzed are very similar. This implies (compare figures 3.1 and 3.2) that Chinnery's uniform slip model, even though it has a singularity at the bottom edge of the dislocation surface, is a fair approximation to the

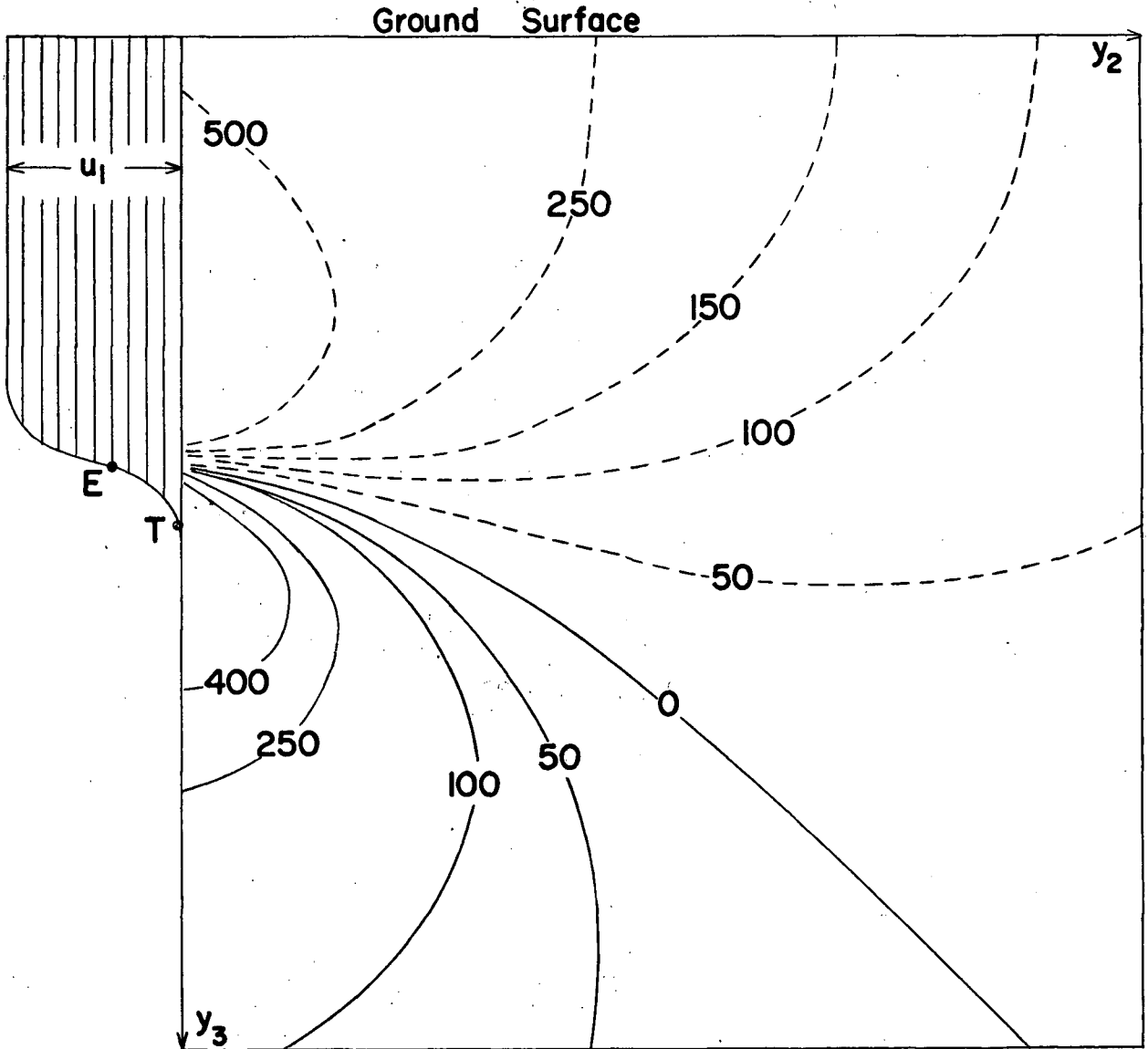


Figure 3.6

Contour map of the τ_{12} component of the stress change in the vertical plane $y_1 = 0$. Contour units are 10^5 dynes/cm².

----- Negative

_____ Positive

Model A

U = 5m

L = 100 km

d = 0

E = 10 km

T = 12 km

$\mu = 3 \times 10^{11}$ cgs

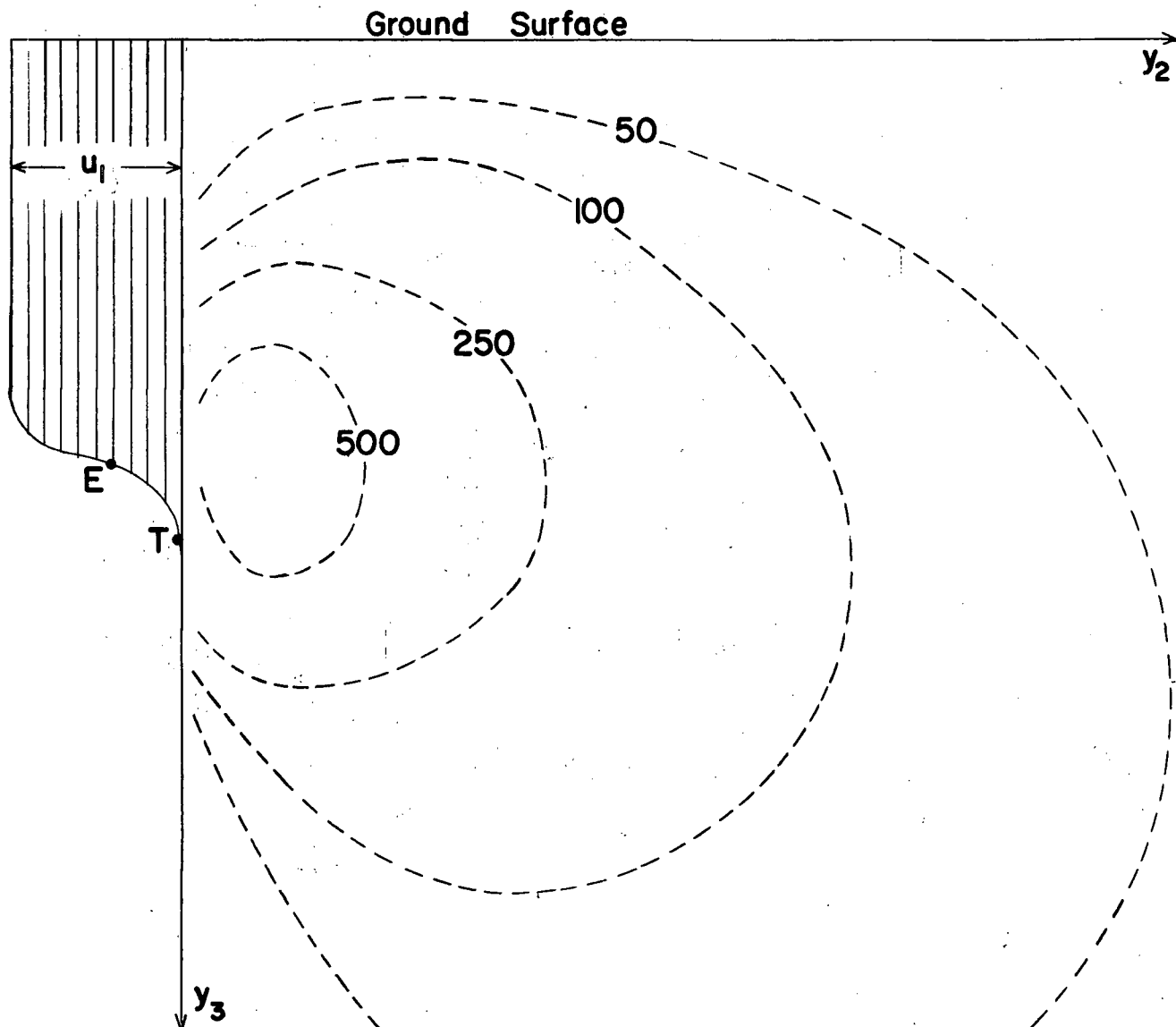


Figure 3.7

Contour map of the τ_{13} component of the stress change in the vertical plane $y_1 = 0$. Contour units are 10^5 dynes/cm².

----- Negative

Model A

$U = 5$ m

$L = 100$ km

$d = 0$

$E = 10$ km

$T = 12$ km

$\mu = 3 \times 10^{11}$ cgs

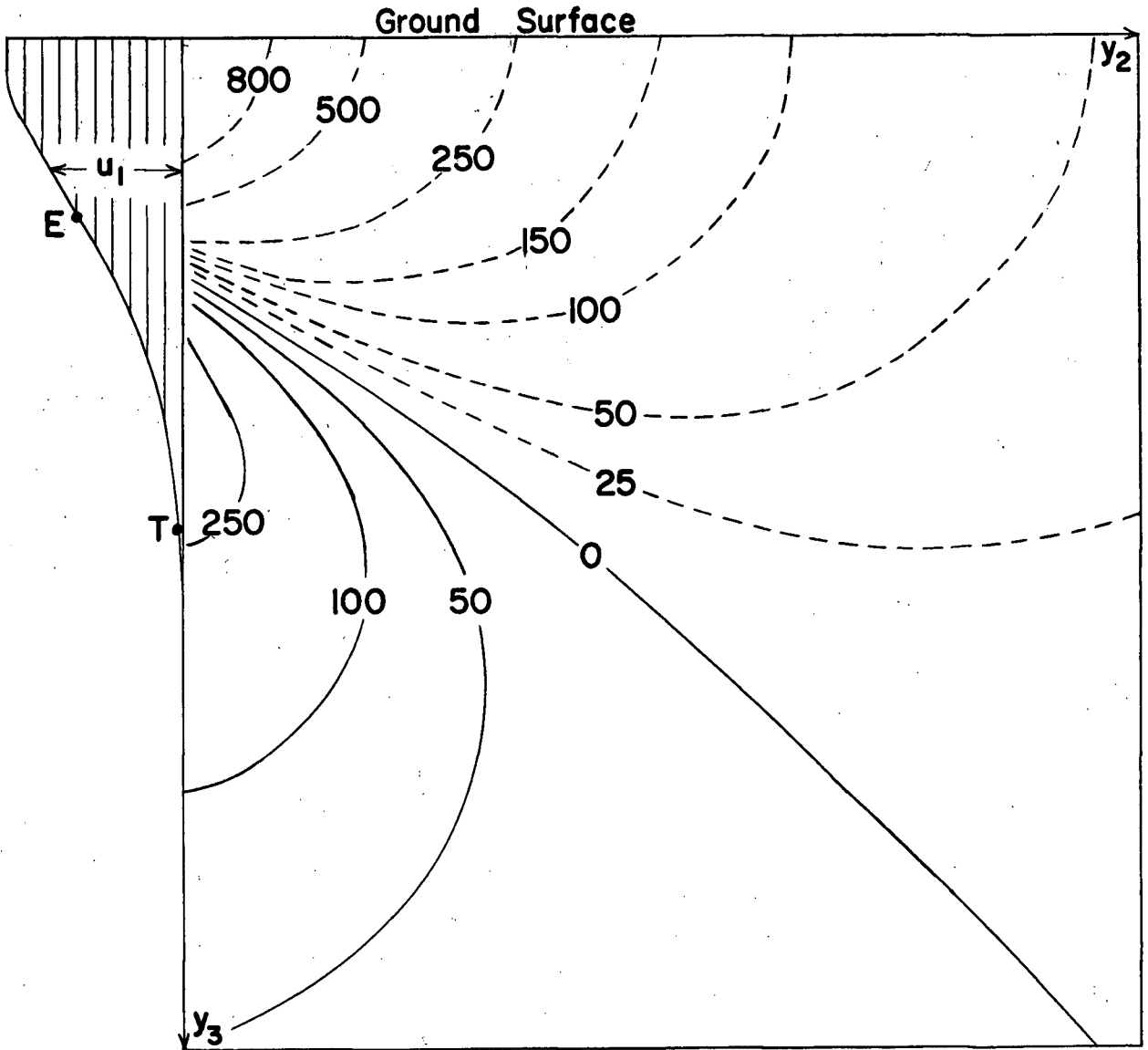


Figure 3.8

Contour map of the τ_{12} component of the stress change in the vertical plane $y_1 = 0$. Contour units are 10^3 dynes/cm².

----- Negative

_____ Positive

Model B

$U = 5$ m

$L = 100$ km

$d = 0$

$E = 6$ km

$T = 11$ km

$\mu = 3 \times 10^{11}$ cgs

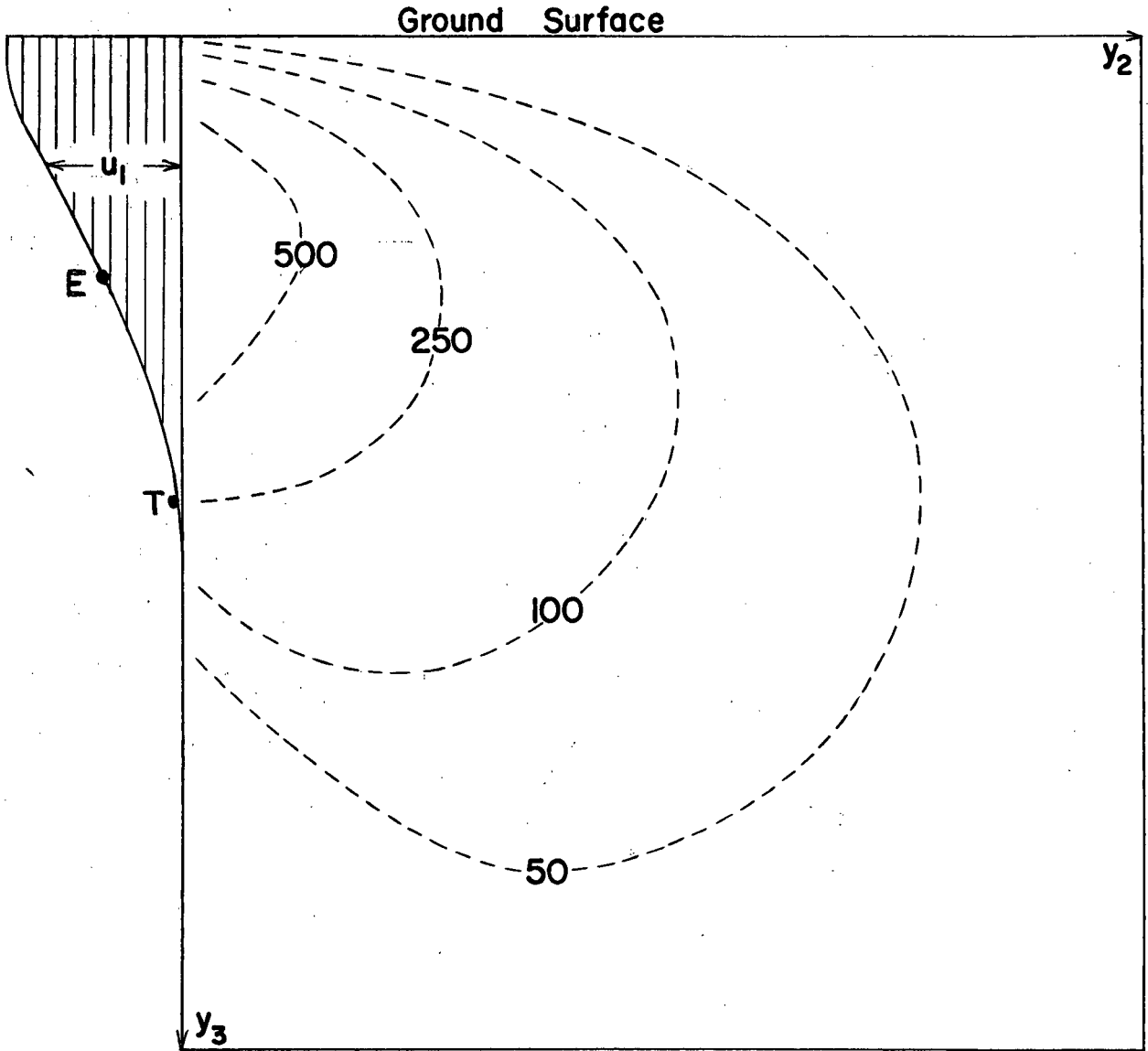


Figure 3.9

Contour map of the τ_{13} component of the stress change in the vertical plane $y_1 = 0$. Contour units are 10^5 dynes/cm².

Model B

$U = 5$ m

$L = 100$ km

----- Negative

$d = 0$

$E = 6$ km

$T = 11$ km

$\mu = 3 \times 10^{11}$ cgs

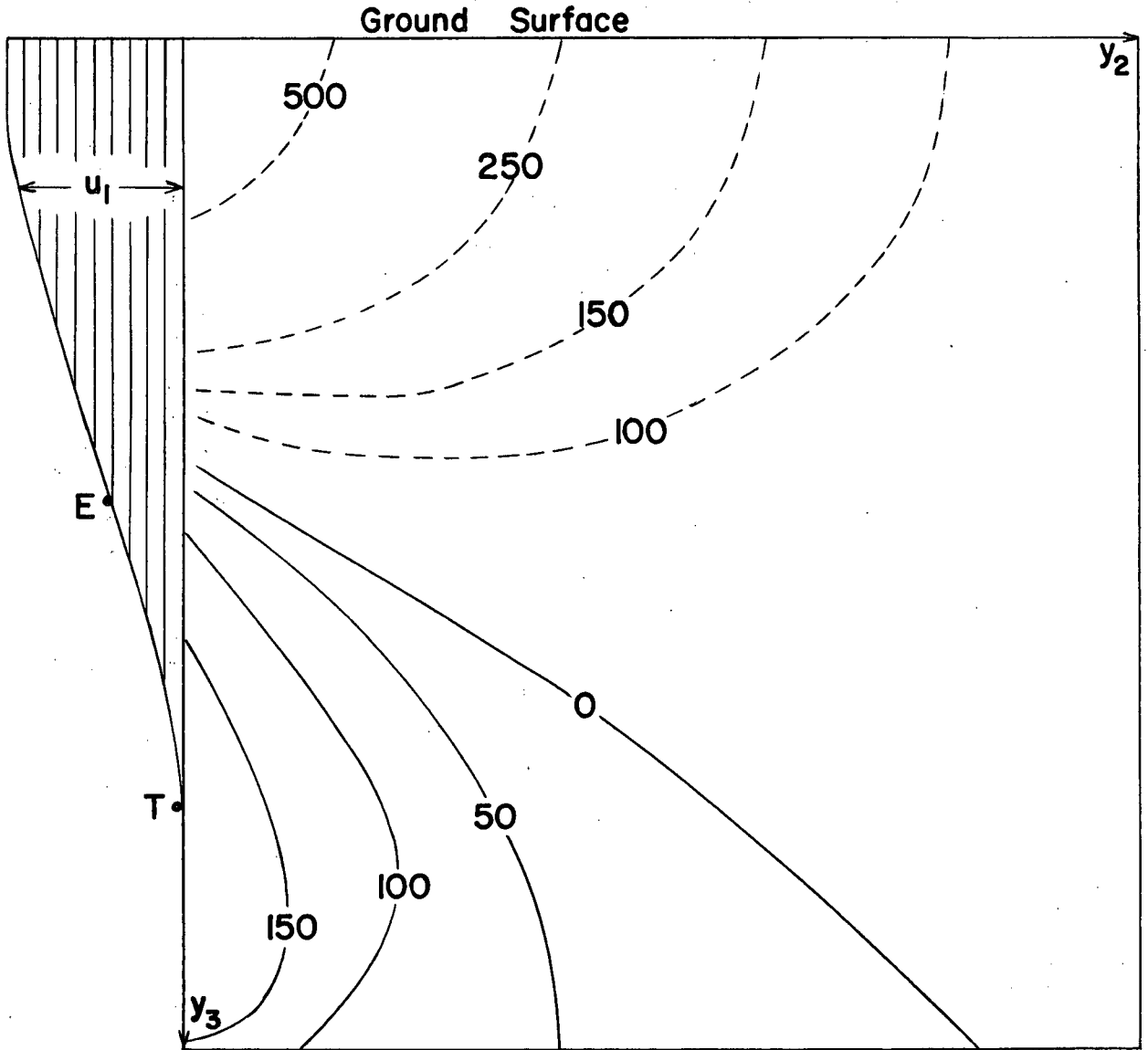


Figure 3.10

Contour map of the τ_{12} component of the stress change in the vertical plane $y_1 = 0$. Contour units are 10^5 dynes/cm².

----- Negative
_____ Positive

Model C
U = 5 m
L = 100 km

d = 0
E = 10 km
T = 16 km
 $\mu = 3 \times 10^{11}$ cgs

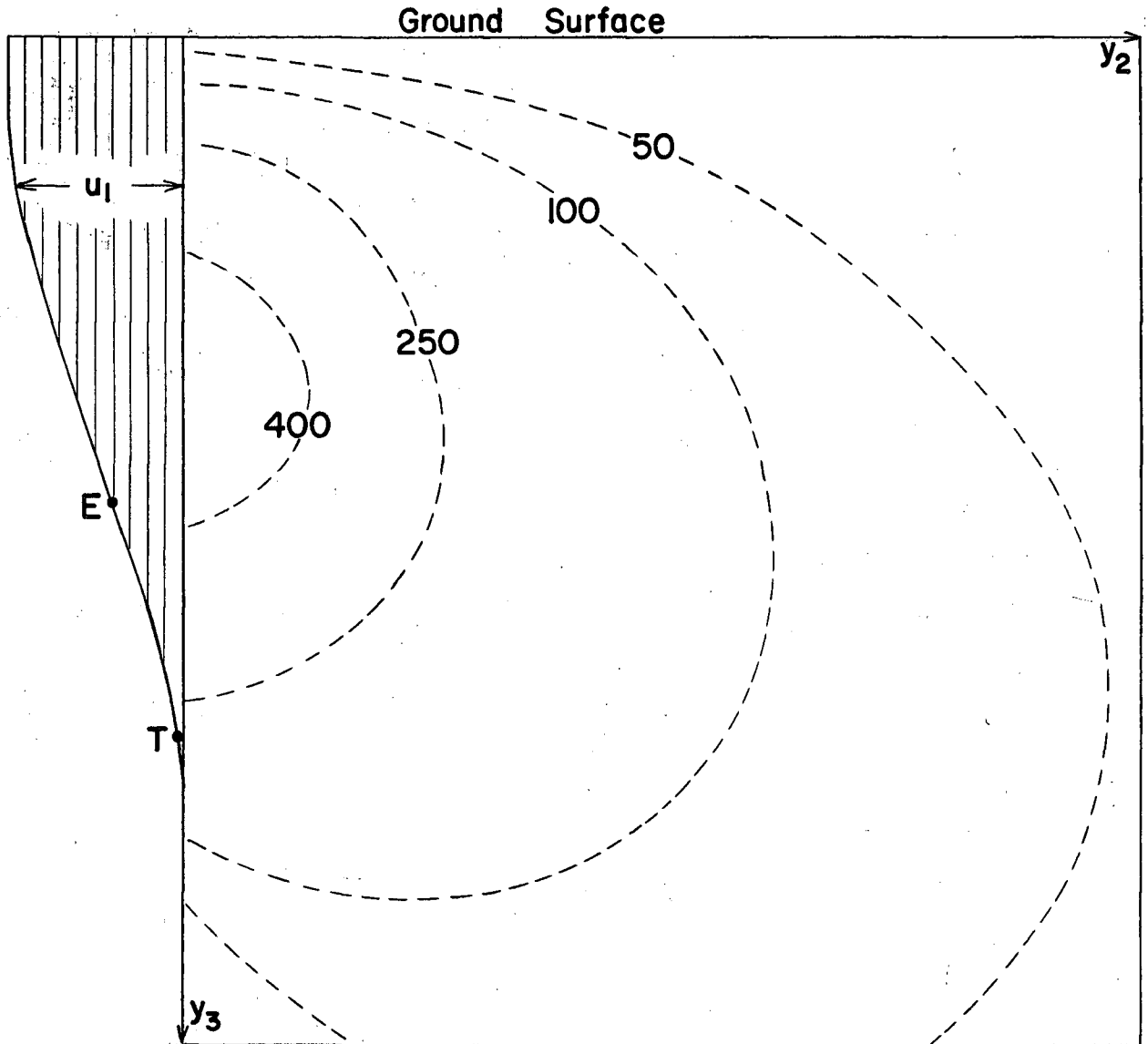


Figure 3.11

Contour map of the τ_{13} component of the stress change in the vertical plane $y_1 = 0$. Contour units are 10^5 dynes/cm².

----- Negative

Model C

U = 5 m

L = 100 km

d = 0

E = 10 km

T = 16 km

$\mu = 3 \times 10^{11}$ cgs

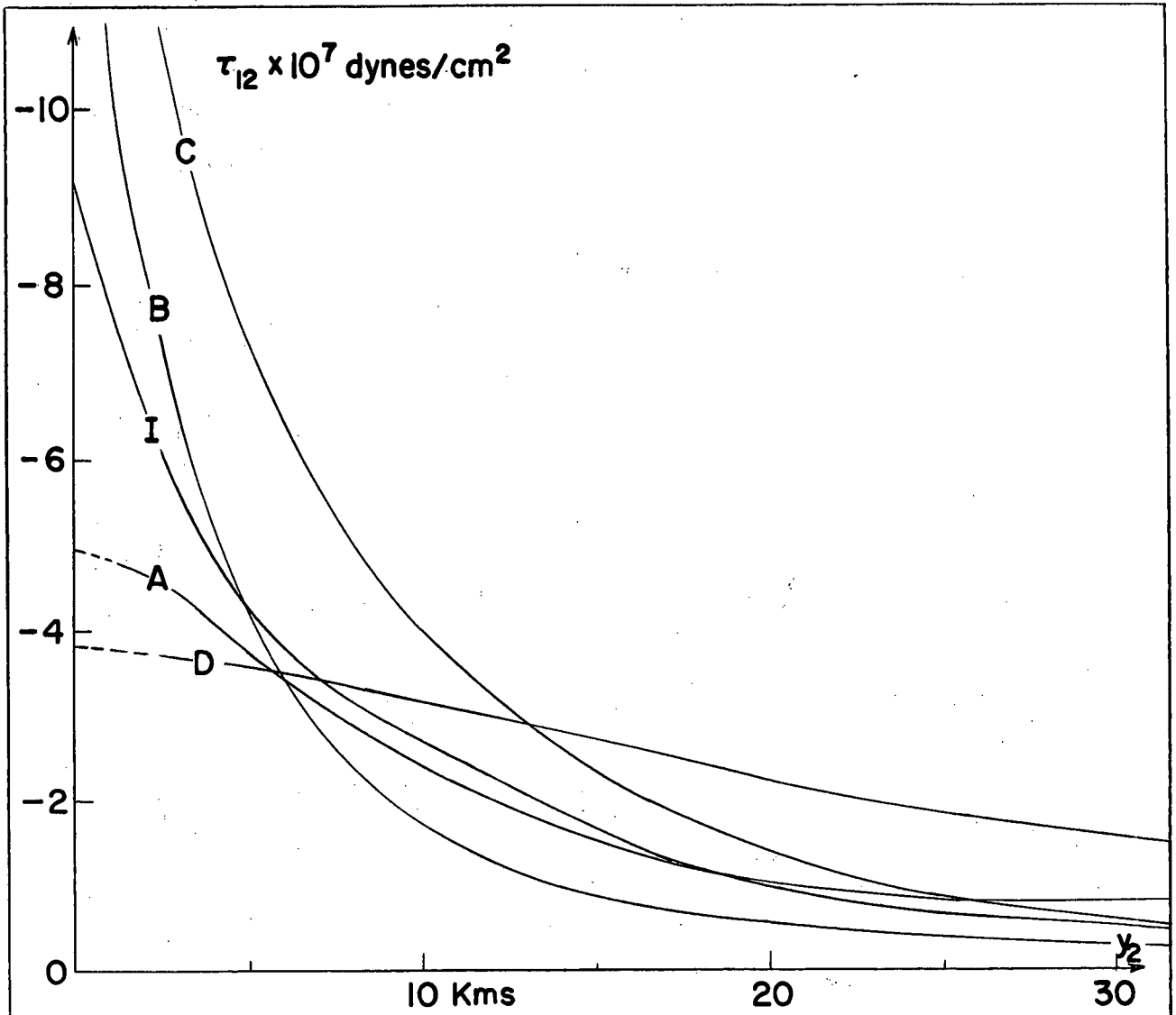
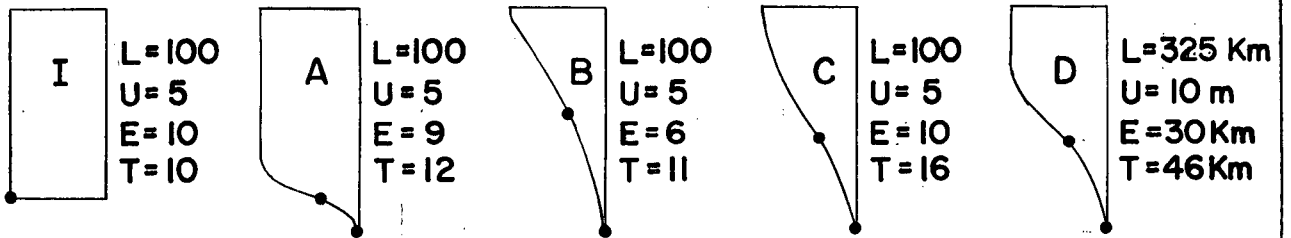


Figure 3.12

Dislocation Surfaces



Fall-off of the τ_{12} stress component with y_2 at the surface of the medium ($y_3 = 0$), along $y_1 = 0$.

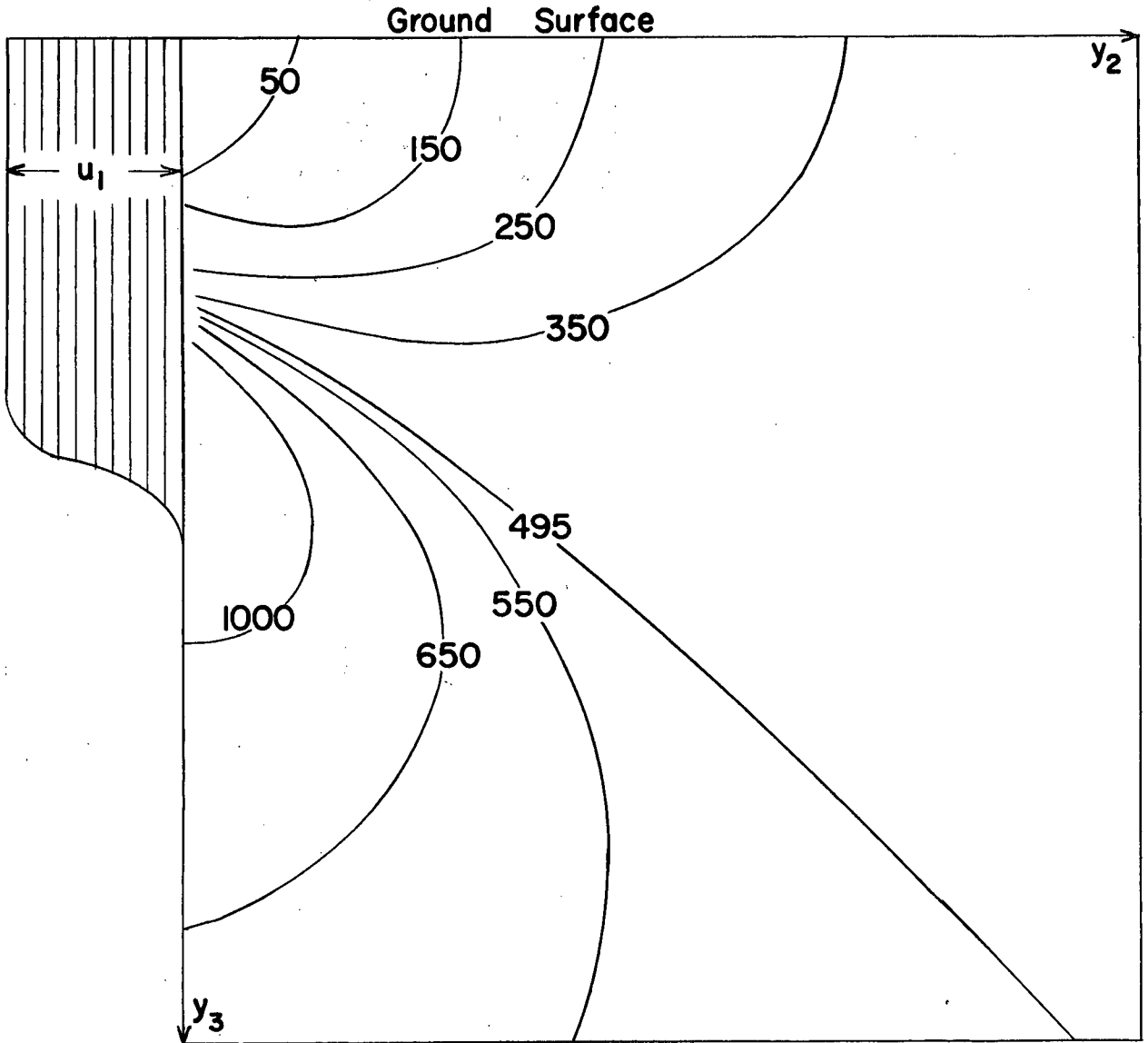


Figure 3.13

Contour map of the magnitude of the maximum shear stress in the vertical plane $y_1 = 0$. Contour units are 10^5 dynes/cm².

$$\text{Stress release } \tau_{12}^0 = 4.95 \times 10^7 \text{ dynes/cm}^2$$

Model A

$U = 5$ m

$L = 100$ km

$d = 0$

$E = 10$ km

$T = 12$ km

$\mu = 3 \times 10^{11}$ cgs

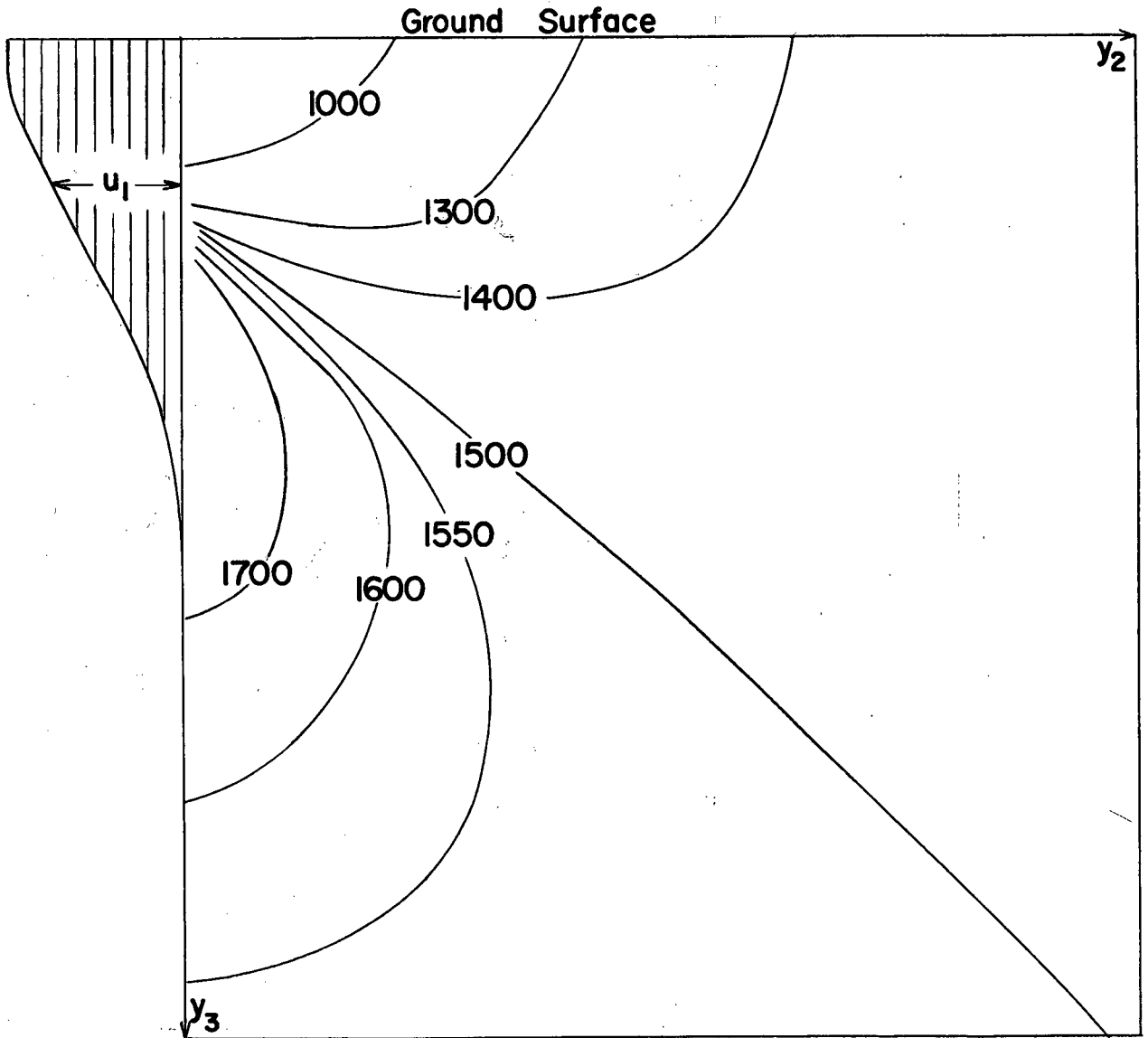


Figure 3.14

Contour map of the magnitude of the maximum shear stress on the vertical plane $y_1 = 0$. Contour units are 10^7 dynes/cm².

Stress release $\tau_{12}^0 = 1.5 \times 10^8$ dynes/cm².

Model B

$d = 0$

$U = 5$ m

$E = 6$ km

$T = 11$ km

$L = 100$ km

$\mu = 3 \times 10^{11}$ cgs

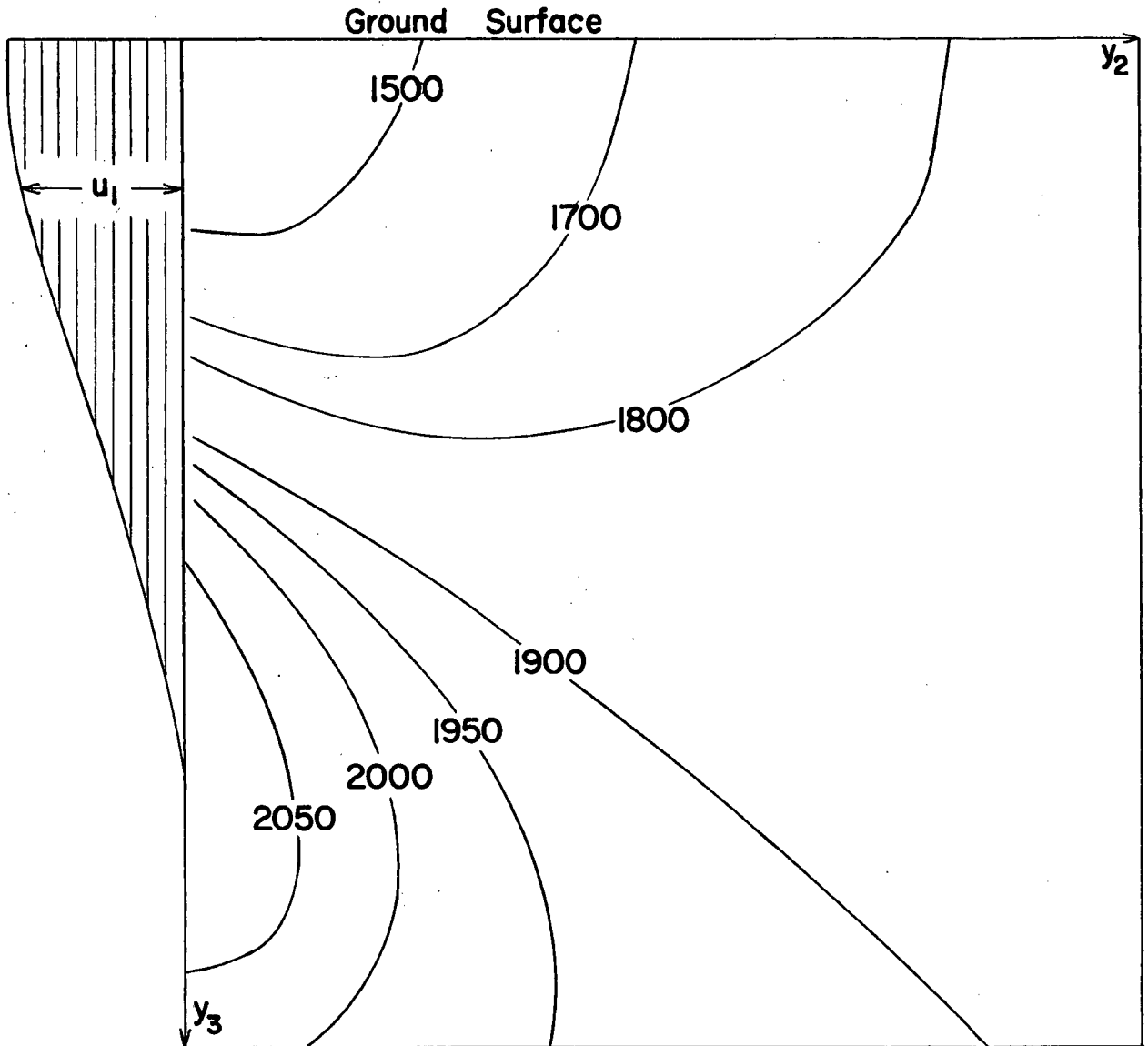


Figure 3.15

Contour map of the magnitude of the maximum shear stress in the vertical plane $y_1 = 0$. Contour units are 10^5 dynes/cm².

$$\text{Stress release } \tau_{12}^0 = 1.9 \times 10^8 \text{ dynes/cm}^2$$

Model C

$$d = 0$$

$$U = 5 \text{ m}$$

$$E = 10 \text{ km}$$

$$T = 16 \text{ km}$$

$$L = 100 \text{ km}$$

$$\mu = 3 \times 10^{11} \text{ cgs}$$

more physically reasonable variable slip model. In figure 3.2 we have removed the singularity by applying a variable-slip discontinuity in this unstable region only to find results that are almost identical to those of Chinnery. Figure 3.5, however, shows clearly that some differences exist in the rate of fall-off of the horizontal displacements for each of the cases considered. Indeed, this characteristic proves very useful in our depth analyses of several faults as discussed in chapter 4.

The depth described by Chinnery's model is definitely a fixed value. However, this is not the case for the variable-slip models A, B, and C where there are two values of the depth which are of consequence. These are the effective depth (E) and the total depth (T) of the fault. The effective depth (compare figures 3.1, 3.2, and 3.4) shown in figure 3.4 corresponds identically with the total depth T of Chinnery's model and the effective depth E of model A. Also, the contours and the rate of fall-off of horizontal displacement for each of these three cases are very similar to one another. The same observations, however, do not apply to model B which was constructed so that its total depth would correspond to the total depth of Chinnery's model and the

effective depth of models A and C. In model B the horizontal displacement, u_1 , falls off more rapidly than in any of the other cases. Also, its contours are considerably shallower than those exhibited in figures 3.1, 3.2 and 3.4.

With these considerations in mind we propose that the fault depths determined by Chinnery (1962) approximate only the effective depths and not the total depths of any given dislocation surface i.e. the values calculated by Chinnery are approximately 50% too shallow.

In this section we have used only a hypothetical fault to support our argument. Chapter 4, however, contains the depth analyses of five actual dislocation surfaces and a table (4.1) listing depth estimates by Kasahara (1958) and Chinnery (1961, 1962) as well as our new estimates determined using a variable-slip model.

3.10 Results of the Stress Analyses

Contour maps of the τ_{12} and τ_{13} components of the stress change in the plane $y_1 = 0$ are exhibited in figures 3.6 - 3.11 for models A, B, and C. A close examination of figures (3.6, 3.8, 3.10) and figures (3.7, 3.9, 3.11) shows that the shapes of the contours in each case are very similar. On the other

hand, figure 3.12 clearly indicates that vast differences in the rate of fall-off of the τ_{12} stress component do exist. This means that the stress release at the origin, τ_{12}° , which we assume was the stress causing the fracture to occur, varies considerably from one fault model to another. Furthermore, extremely high values of τ_{12}° may imply that the corresponding fault models are physically unfeasible.

It is interesting to note that figures (3.6, 3.8, 3.10), respectively, show a positive stress distribution of diminishing magnitude about the bottom of the fault in the plane $y_1 = 0$. The fact that this distribution is a positive one indicates immediately that the fault will have a tendency to propagate downwards in an effort to relieve the existing stress.

A brief examination of each of the models displayed indicates two trends: (1) a gradual decrease of slip with depth is associated with a positive stress distribution (τ_{12}) of smaller magnitude, (2) for deeper fractures, much of the stress must have been relieved in the process of downward propagation. This would explain the relationship between the slip, depth, and positive (τ_{12}) stress component for the models discussed. Contours of the stress change τ_{13} are shown

here for the sake of completeness and because they are required in the calculation of the maximum shear stress.

A physically more meaningful quantity, the maximum shear stress, has been calculated in the plane $y_1 = 0$ for models A, B, and C. Contour maps for each of these models are exhibited in figures 3.13 to 3.15. They display shapes very similar to those of the τ_{12} stress component and are divided into two basic regions. These are the region of stress relief which borders the ground surface and the region stressed above the breaking strength of the medium (the breaking strength is the theoretical approximation τ_{12}^0). The latter is centred about the fault base in a zone in which after-shock activity is often recorded.

Based on the above ideas, we propose that a vertical strike-slip fault will tend to propagate downwards in order to relieve the positive stress about its base. In chapter 5 we attempt to associate the after-shock zone of an actual earthquake with the aforementioned region of high stress.

CHAPTER 4

A COMPARISON OF THE THEORETICAL DISPLACEMENT FIELD
WITH OBSERVATIONS

We shall now apply the general analyses of the previous chapter to the displacements of the ground observed around five surface faults.

Of course no real fault corresponds exactly with any theoretical model. There will always be topographic features, inhomogeneities in the surrounding medium, inaccurate measurements of the various fault parameters, and several other factors (see Chapter 1.3) that will prevent us from simulating an accurate reproduction of the actual physical conditions.

Hence, in the following discussion we shall try to fit the geodetic data with several reasonable theoretical approximations rather than attempt to give a single interpretation.

4.1 The Source of Geodetic Data

The horizontal displacements of triangulation points around an earthquake fault provide valuable information about the physical conditions of the fault-

ing. Here we apply the dislocation theory of a variable-slip, strike-slip fault to some actual cases in order to determine their probable depths. The following analyses pertain to the San Andreas fault, the Gomura fault, the Tanna fault, the Imperial Valley fault, and the Fairview Peak fault. Geodetic data for each of these have been reported in considerable detail by several authors.

4.2 The San Francisco Earthquake

The San Francisco earthquake of April 18, 1906, is associated with a long shallow fracture known as the San Andreas fault. This fault is of prime interest to us, not only because it is straight and displays very little vertical movement, but also because accurate triangulations were made to determine the displacements of the ground around it. Two surveys are relevant to the actual fracture - that of 1868 before the fracture zone existed and the resurvey (only 47 triangulation points) after the fracture occurred. A plot of the geodetic data, given in figure 4.1, shows that this time interval of about thirty-eight years has been long enough for a considerable amount of strain to accumulate in the region. However, other small regional faults, the nearby sea, and inhomogeneities in the

medium should also be considered as factors contributing to the more or less random movement of the ground surface.

4.3 The Tango Earthquake

The Tango earthquake occurred on March 7, 1927 on the northern coast of central Japan. The two fractures produced at this time were the Yamada and the Gomura faults. Our interest lies only in the latter for which 273 triangulation points were resurveyed. Some of this data have been plotted in figure 4.2 together with an elevated base line which has been attributed to the block movements that have occurred during the time interval between surveys (about 30 years). Such activity and also some dip-slip movement (about 0.7 meters) imply that this fault departs considerably from the idealized dislocation surface that we have been discussing. However, appropriate adjustments may be made so that our analysis using dislocation theory is applicable.

4.4 The North Izu Earthquake

The North Izu earthquake occurred on November 26, 1930 in the northern part of the Izu Peninsula off the southern coast of Japan. The Tanna fault, a

vertical but slightly convex (to the East) fracture was associated with this earthquake. In the vicinity of the fracture, 81 triangulation points were surveyed and resurveyed during the seven year interval between the time of the Great Kwanto earthquake of 1923 and the above event of 1930. The measured differences are assumed to be due entirely to the Tanna fault although there is no way of determining whether or not other seismic activity in the surrounding area was a contributing factor to the movements. This data has been plotted in figure 4.3 so that it may be compared with the displacements obtained using a theoretical model.

4.5 The Imperial Valley Earthquake

A plot of the movements of the triangulation stations on either side of the Imperial Valley fault of May 18, 1940 were taken from a map prepared by C. A. Whitten (1949) of the Coast and Geodetic Survey. Kasahara's (1958a) interpretation of this map shows a decrease of horizontal displacement, u , with distance from the fault. The geodetic points used by Kasahara have been plotted in figure 4.4. It is important to note that the fall-off is considerably different on the two sides of the fracture. This would indicate

that the fault dips steeply (to the East). As a result, depths obtained from the data on each side of the fracture must be averaged before a meaningful value can be determined.

4.6 The Nevada Earthquake

On December 16, 1954 two earthquakes about four minutes apart shook the neighbourhood of the Dixie Valley, Nevada. Associated with the largest shock was the Fairview Peak fault which displayed both vertical movement and a dip (to the East) as well as a large horizontal slip. Scarps caused by the faulting and many minor fractures were also present in the immediate vicinity. This activity was sufficient to obscure the trace of the main fault so badly that it could be determined only roughly from the movements of the triangulation stations. The latter were presented by Whitten (1957) and interpreted by Kasahara (1958a). Once again the fall-off of horizontal displacement, u_1 , (see figure 4.5) varies considerably on each side of the fracture and thus requires that we make suitable compensation when calculating the depth. The fall-off discrepancy has been attributed to a dip of the fault plane at an angle of $62\frac{1}{2}^{\circ}$ to the East (Romney 1957).

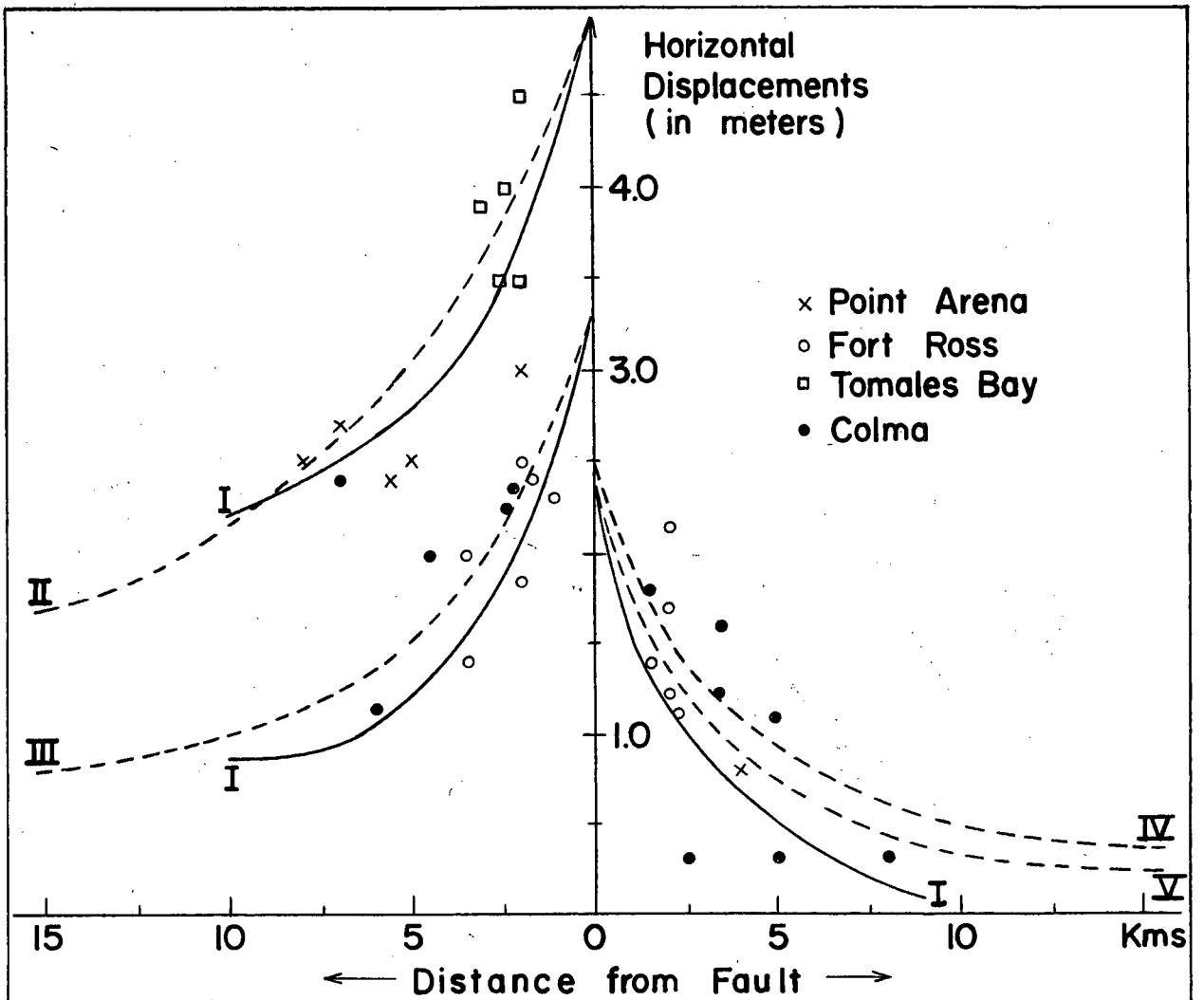
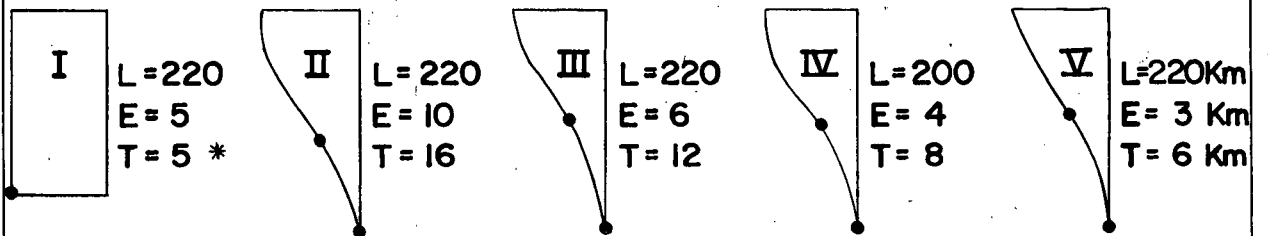


Figure 4.1
Dislocation Surfaces



* Average Value

———— Chinnery 1959

----- Petrak 1965

Fall-off of horizontal displacement with distance in the San Francisco Earthquake.

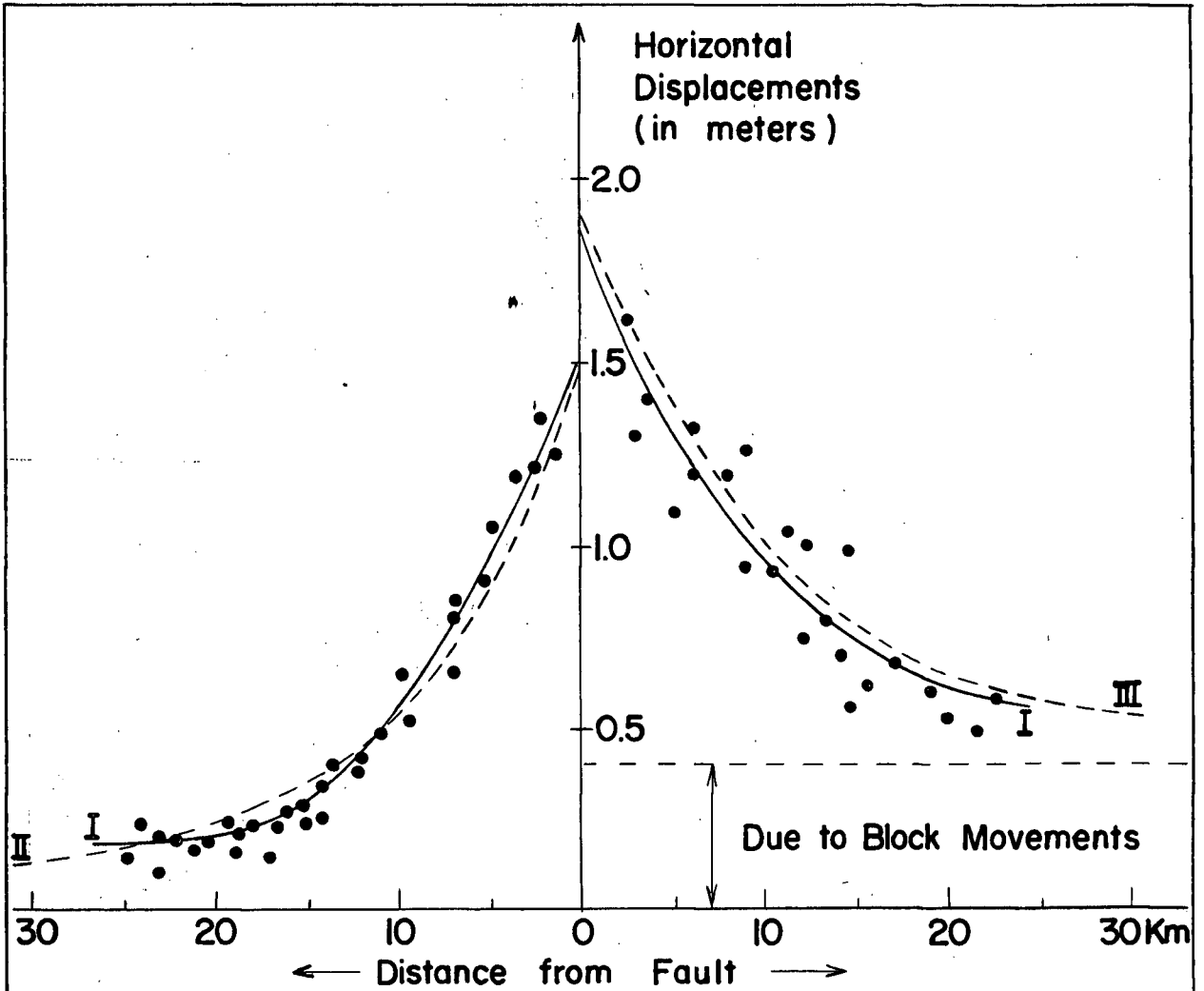
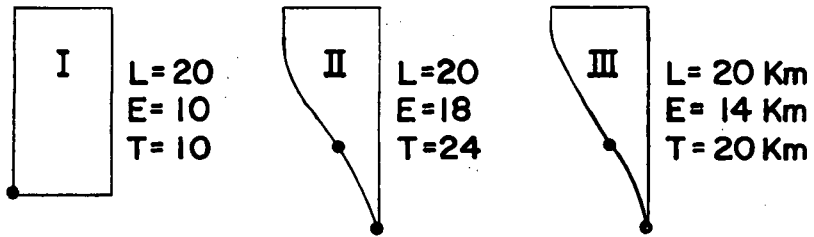


Figure 4.2

Dislocation Surfaces



— Chinnery 1959
- - - - - Pettrak 1965

Fall-off of horizontal displacement with distance in the Tango Earthquake.

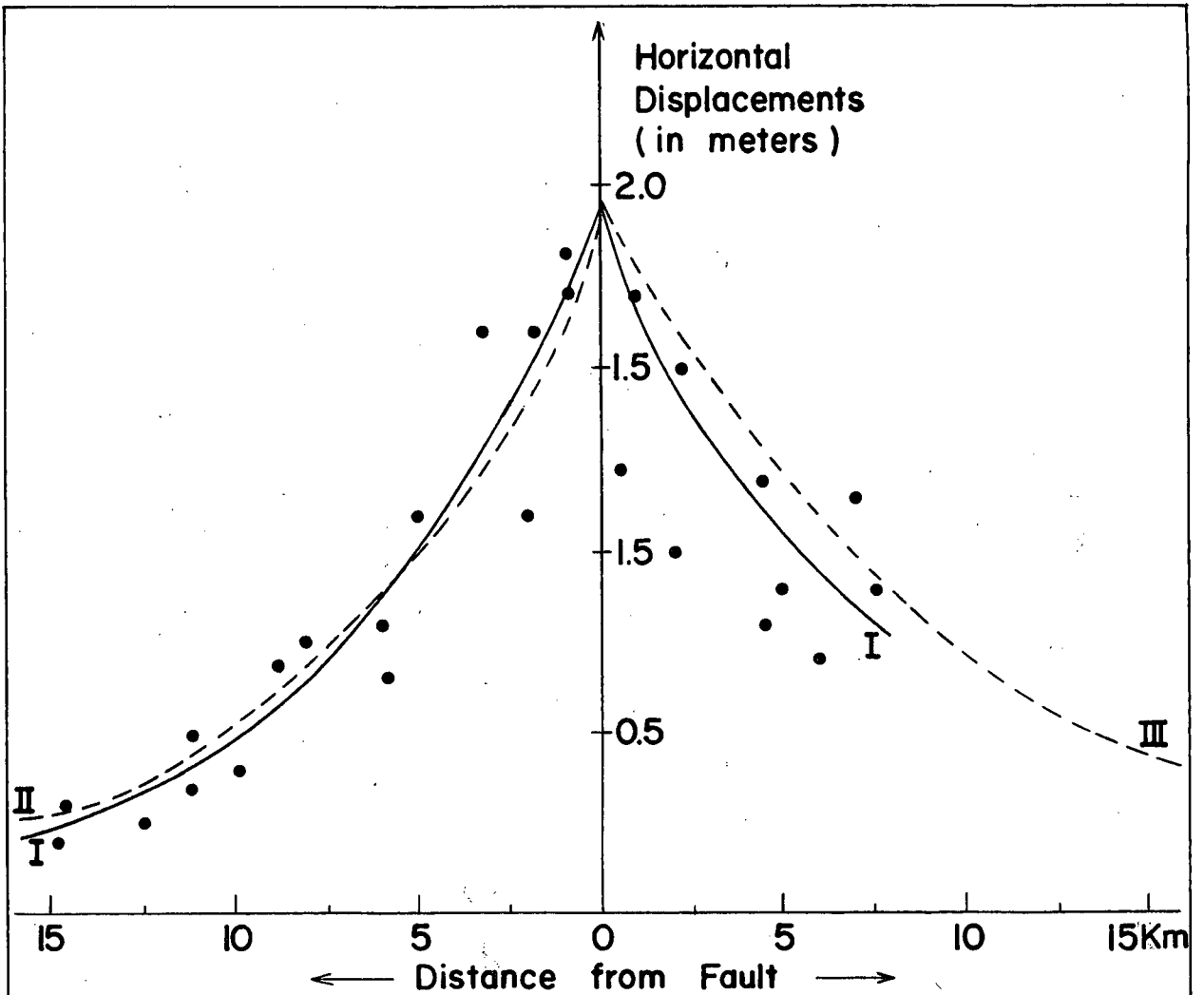
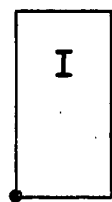
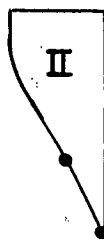


Figure 4.3

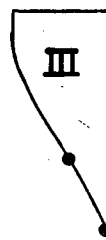
Dislocation Surfaces



I
L=12
E=12
T=12



II
L=12
E=20
T=26



III
L=15 Km
E=20 Km
T=26 Km

———— Chinnery 1959
----- Petrak 1965

Fall-off of horizontal displacement with distance in North Izu Earthquake.

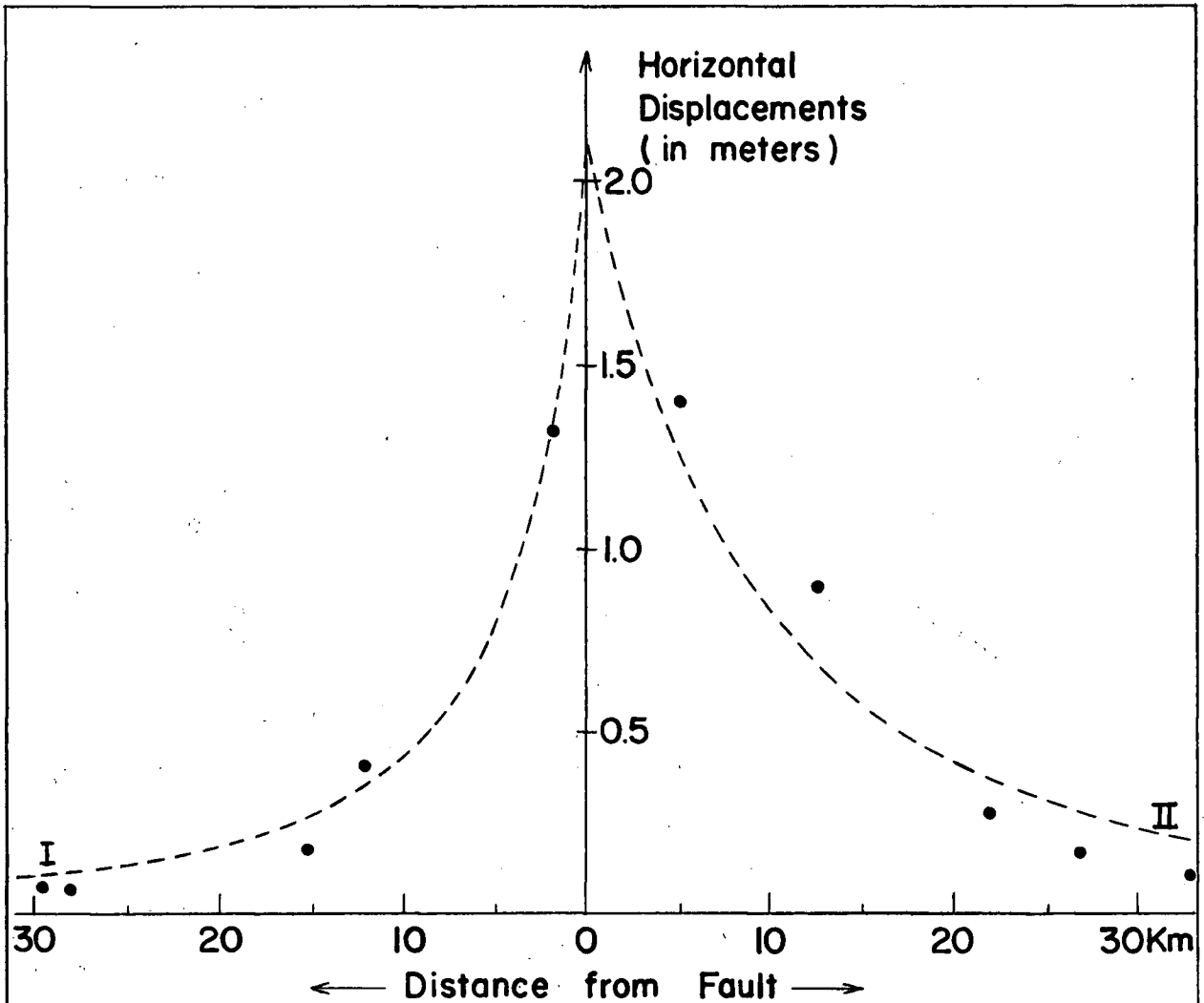
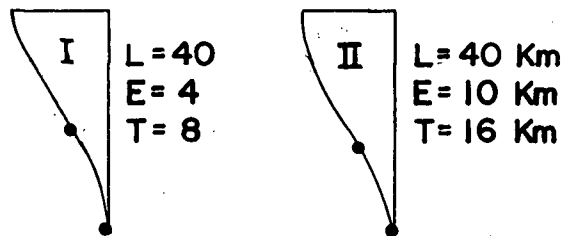


Figure 4.4

Dislocation Surfaces



----- Petrak 1965

Fall-off of horizontal displacement with distance in the Imperial Valley Earthquake.

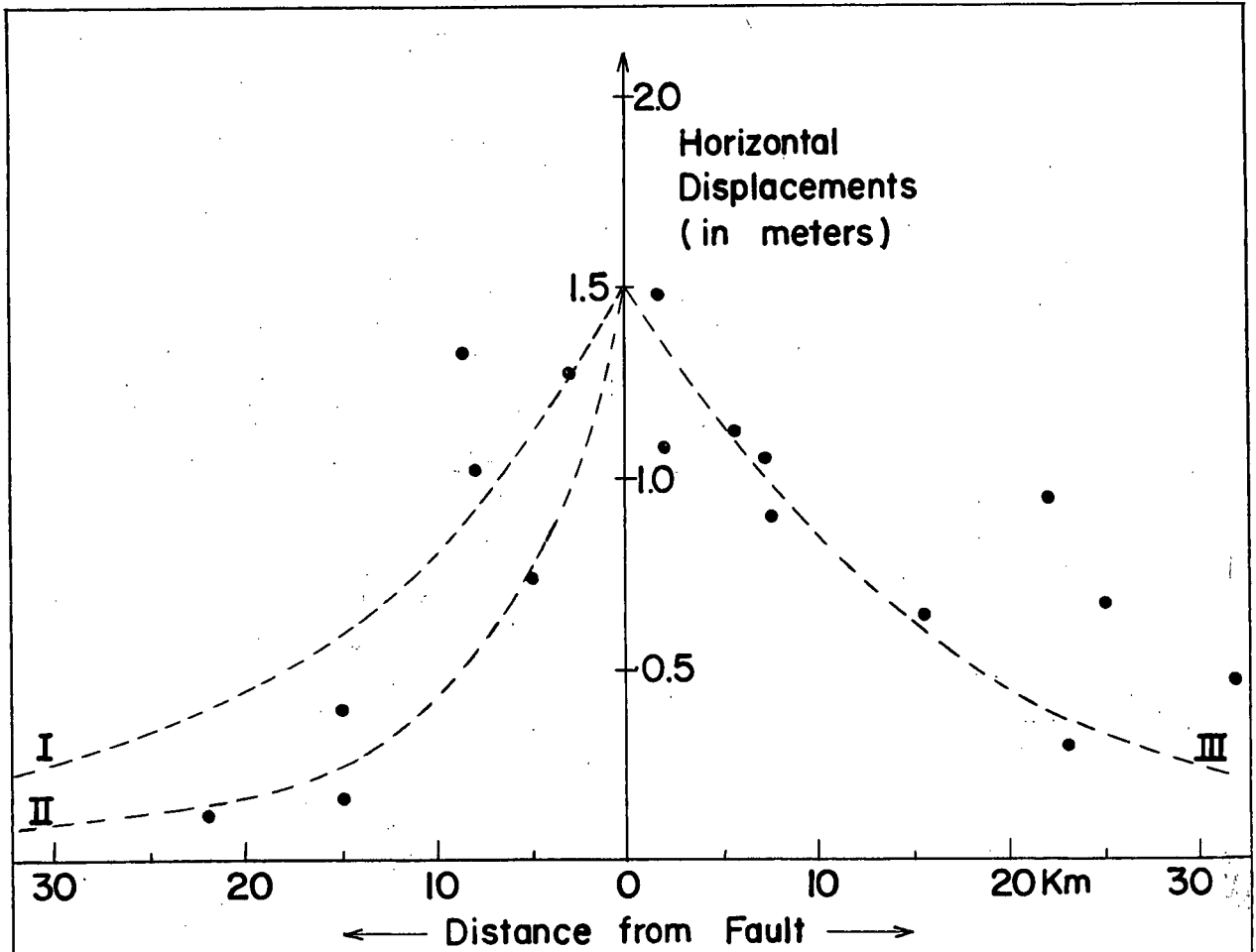
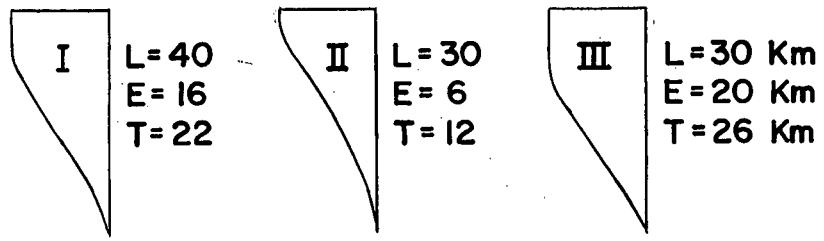


Figure 4.5

Dislocation Surfaces



----- Petrak 1965

Fall-off of horizontal displacement with distance in the Nevada Earthquake.

4.7 Application of Theory to Observation

When calculating the displacements using dislocation theory, each change in the fault dimensions produces some noticeable change in the analytical results. Such an approach is the only way we have of determining any trends or characteristics exhibited by a given fault model. In such analyses the mathematician rarely concerns himself with the accuracy of the geodetic data which he uses as a basis for his model. Rather, he tends to become completely involved in an examination of the theoretical results.

This situation was not allowed to develop in our analyses of the various fault models. Care was taken to remember that such parameters as the fault semi-length L and its slip U can be measured only approximately in the field. For instance, in resurveying the ground surface a base line must be chosen on the assumption that it has not been affected by the disturbance. This of course is never justified since the resurvey must include the area very close to the fracture. As a result, errors in both the magnitude and the direction of the observed displacements must be expected.

The measurements of the length $2L$ of some of the five surface faults examined were only rough estimates. For example, it has been suggested that the San Andreas fault actually extends north-westwards into the Pacific, and that the Imperial Valley fault may extend well into Mexico. The latter idea is supported by the fact that the maximum fault displacement occurs near the Mexican border.

Such discrepancies become evident from a theoretical viewpoint on an examination of the u , fall-off curves produced by a variable-slip model representation of the Tanna fault ($L \sim D$, Kasahara). In this instance, they showed very little similarity to the geodetic results until we increased the length of the model by about 75% (keeping the depth constant), indicating that a gross error in the measurement of the length, $2L$, of the fault is inherent in the data. Such a situation is indicative of some of the problems that arise in a comparison of theory with observation. To make these matters even more confusing, we have no means of obtaining actual depth measurements of any dislocation surface located in the earth's crust.

4.8 Interpretation of the Fall-off Curves

In figures 4.1 - 4.5 we have superimposed on the geodetic data several theoretical fall-off curves. Among these (figures 4.1 - 4.3) are the approximations of Chinnery (1959) calculated from his constant-slip model. No discussion of actual depth measurements will be given in this section. They have been listed, however, in table 4.1 along with previous estimates prepared by Chinnery (1962) and Kasahara (1958).

From a general analysis of the trends exhibited in figures 4.1 - 4.5, several changes in depth estimates are evident. Those values approximated by Chinnery (1962) are generally 40 - 60% less than our effective fault depths and about 100% less than our total depths. These discrepancies are to be expected, however, since the constant slip model does involve the movement of ^{the} most ground. Kasahara (1958), on the other hand, has produced estimates (except in the case of the Tanna fault) equivalent to our effective depths. Such similarities are not surprising because Kasahara's model, as our own, exhibits displacements which fall off with depth. Those depths suggested for the San Andreas, Imperial Valley, and Fairview Peak faults by Byerly and De Noyer (1958) (their calculations were based on a consideration of

Fault	Kasahara (1958)				Dislocation Theory (Chinnery, 1962)						Dislocation Theory (Petrak, 1965)				
	Slip $u/2$ m	Length $2L$ km	Depth D km	Stress Release τ_{12}^0 $\mu=5 \times 10^{10}$ cgs	Slip $u/2$ m	Length $2L$ km	Depth D km	Stress Release τ_{12}^0 $\mu=3 \times 10^{10}$ cgs	Stress Release τ_{12}^0 $\mu=5 \times 10^{10}$ cgs	Slip $u/2$ m	Length $2L$ km	Effective Depth E km	Total Depth T km	Stress Release τ_{12}^0 $\mu=3 \times 10^{10}$ cgs	
San Andreas (Reid et al, 1908)	2.5	440	6	2.8×10^8	2.5	440	~ 5	9.6×10^7	1.6×10^8	2.5	440	6	12	1.6×10^8	
			*(10)			∞	~ 5								1.6×10^8
Gomura (Tango) (Tsuboi, 1932)	1.5	30	15	5×10^7	1.7	30	15	3.7×10^7	6.2×10^7	1.7	40	19	25	4.1×10^7	
						40	10								6.4×10^7
Tanna (Izu) (Yamaguti, 1937)	2.0	15	8	1.2×10^8	1.9	18	> 50	—	—	1.9	18	> 50	—	—	
						24	12								8.7×10^7
Imperial Valley (Whitten, 1949)	2.1	70	8	1.3×10^8	2.1	70	6	6.8×10^7	1.1×10^8	2.1	70	7	13	8.3×10^7	
			*(80)			∞	6								8.0×10^7
Fairview Peak (Whitten, 1957)	1.5	60	15	5.0×10^7	1.5	45	16	2.4×10^7	4.0×10^7	1.5	45	> 30	—	—	
			*(80)			60	10				5.3×10^7	60			20
			*(23)			80					80	15	21	2.7×10^7	

Table 4.1

* Byerly and DeNoyer

Results of the Model Calculations on Some Real Faults

strain energies and earthquake intensities) agree very well with our total depth estimates in all three cases. However, we have no way of knowing whether or not this agreement is a coincidence or reality, especially since Byerly and De Noyer state "The value of 10 Km was distasteful to us, but the rapid die off of intensity from the fault seems to demand a shallow break" (the reference here is to the San Andreas fault). The similarity of these results to our own remains, nevertheless, and should be investigated further.

CHAPTER 5

A COMPARISON OF THE THEORETICAL STRESS DISTRIBUTION WITH OBSERVATION

In this section we apply the general analyses of Chapter 3 to a specific geodetic situation. The contours of maximum shear stress displayed there lead us to enquire whether or not there is any connection between them and aftershocks. The Rat Island Earthquake (off the Alaskan coast) is used to investigate this possibility. Although no definite results are obtained from this analysis, further work may reveal some matters of interest.

Since the sea covers most of the affected region, the exact position of the fault trace cannot be located. Furthermore, neither the fault type nor its relative dimensions have been measured. Thus the following comparison of theory and observation must be treated as a hypothesis rather than as an exact interpretation of the available geodetic data.

5.1 The Geodetic Data

The U.S. Coast and Geodetic Survey located 870 aftershocks following the Rat Island earthquake

of February 4, 1965. The epicentres (figure 5.1) are located between the axis of the Aleutian trench and the island chain in the region of the Aleutian Island arc and form an approximately rectangular zone about 650 km long and 200 km wide. In this region both temporary and permanent seismograph stations were used to determine the hypocentres of the main shock (about 40 km in depth) and twenty aftershocks. The latter have been plotted in plan along with a hypothetical fault trace on figure 5.2 and in elevation on figures 5.3 and 5.4.

The position of the fault trace drawn on figure 5.2 was not chosen in an arbitrary manner. Rather, aftershock regions displayed by Richter et al. 1958, Tocher 1956, and Plafker 1965 were consulted. Each of these situations showed an array of aftershocks, the position of the main shock, and the relevant fault trace. It was noticed that the aftershock zone was divided in a ratio of about 1:2 with the main epicentre lying not on the fault trace but rather near it at one end of the zone. These observations were then applied to the Rat Island earthquake so that its fault trace could be drawn in a physically significant location. The length and depth of this fracture were assumed to correspond respectively, with the extent of the after-

shock zone and the depth location of the main shock. A horizontal slip, U was then arbitrarily chosen in order to carry out model calculations representative of the geodetic situation.

In figure 5.3 the hypocentres of the twenty aftershocks noted in figure 5.2 have been plotted on top of a contour map of the maximum shear stress in the vertical plane $y_1 = 0$. Calculations of the maximum shear stress were also performed in the planes $y_1 = 0.75L$ and $y_1 = 0.95L$. Significant changes in the contour shapes and positions were noticed only in the latter plane which is illustrated in figure 5.4 along with the twenty hypocentres. Fault models of other depths, slips, and lengths were also examined but the results showed no relevant changes.

5.2 The Relationship Between the Aftershock Zone and Maximum Shear Stress

The contours of maximum shear stress whose magnitudes are greater than the stress release τ_{12}^0 exceed the estimated breaking strength of the surrounding medium (3.83×10^7 c.g.s. in this case). It will be assumed that the downwards propagation of the fracture mentioned in Section 3.10 will tend to release

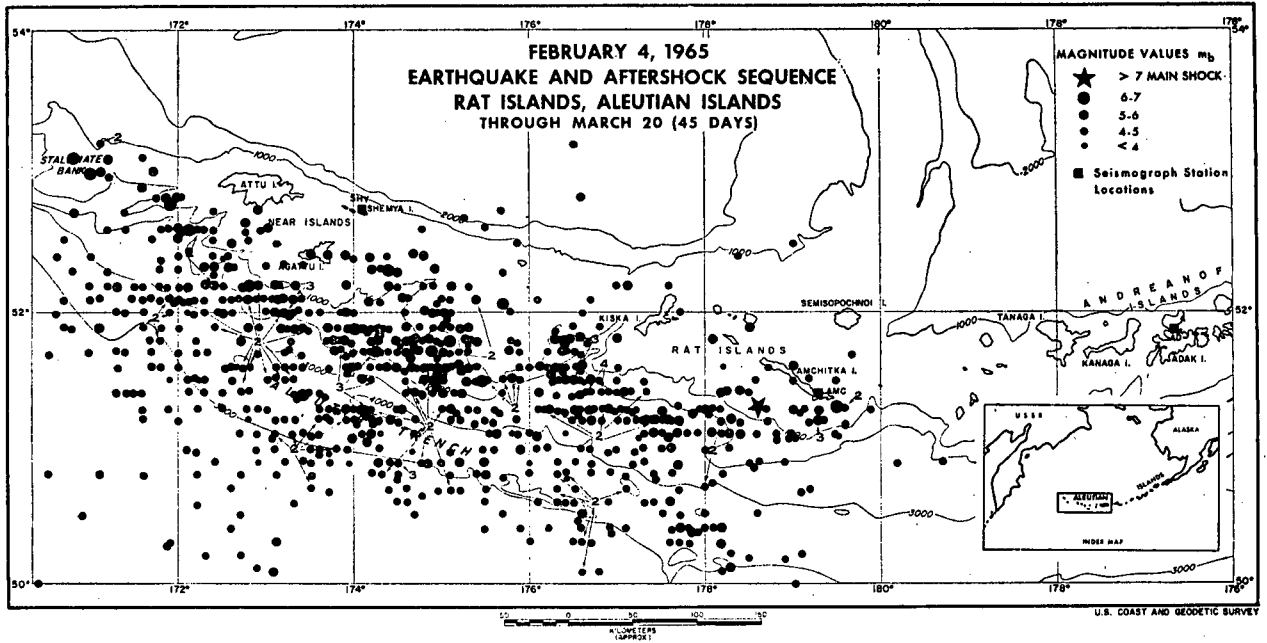


Fig. 5.1 Map of earthquake on 4 February 1965, earthquake and aftershock sequence of the Rat Islands, Aleutian Islands.

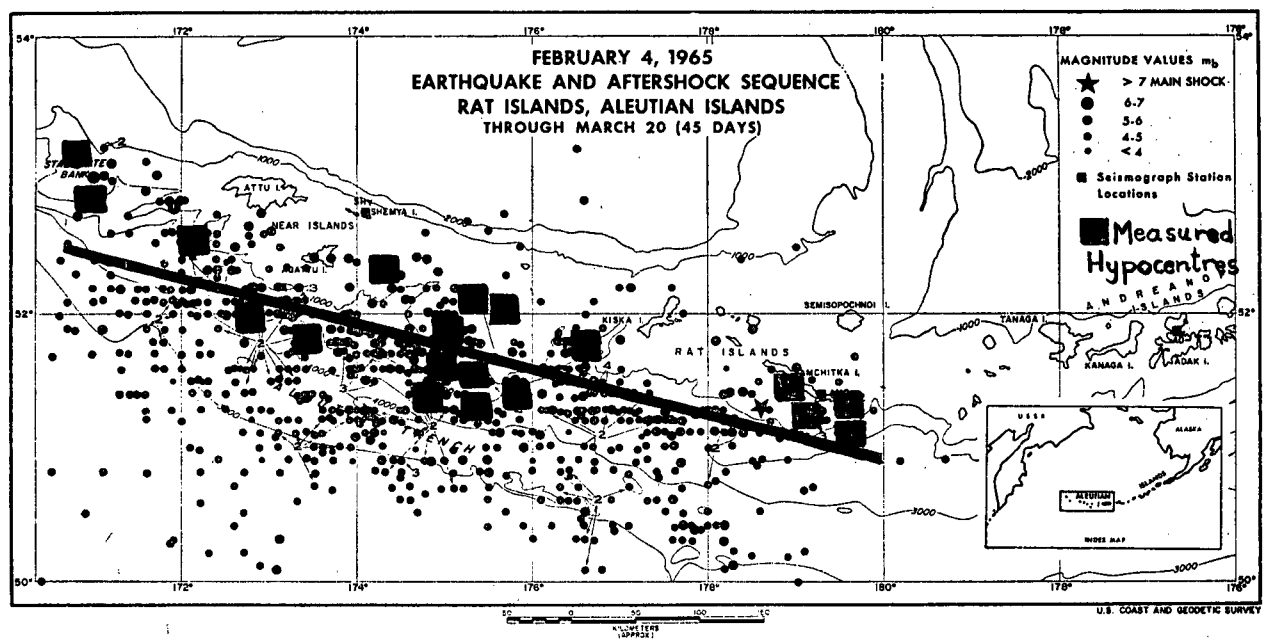


Fig. 5.2 Map of earthquake on 4 February 1965, earthquake and aftershock sequence of the Rat Islands, Aleutian Islands.

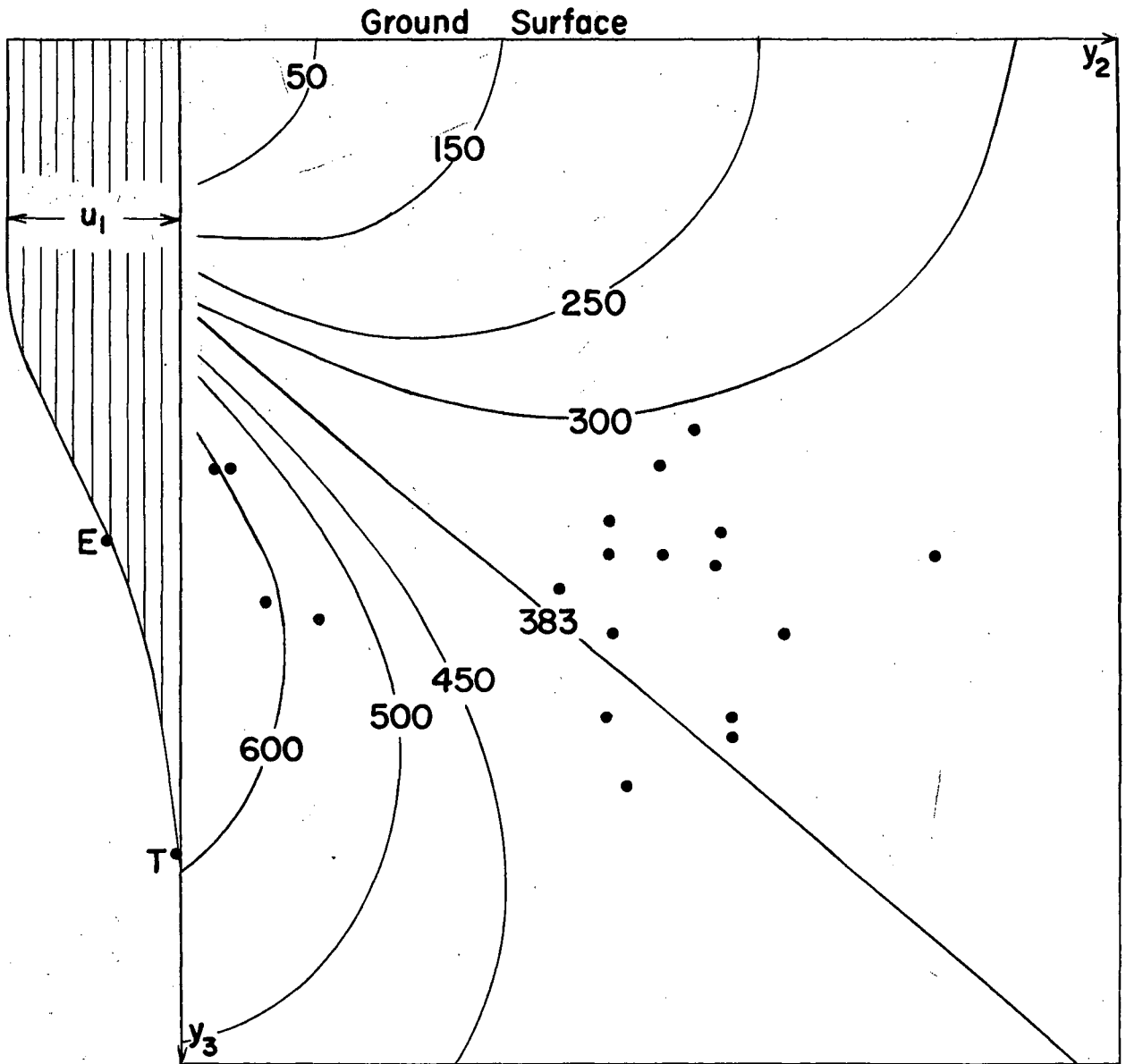


Figure 5.3

Contour map of the magnitude of the maximum shear stress in the vertical plane $y_1 = 0$. Contour units are 10^5 dynes/cm².

Stress release $\tau_{12}^0 = 3.83 \times 10^7$ dynes/cm².

Model D

$U = 10$ m

$L = 325$ km

$d = 0$

$E = 30$ km

$T = 46$ km

$\mu = 3 \times 10^{11}$ cgs

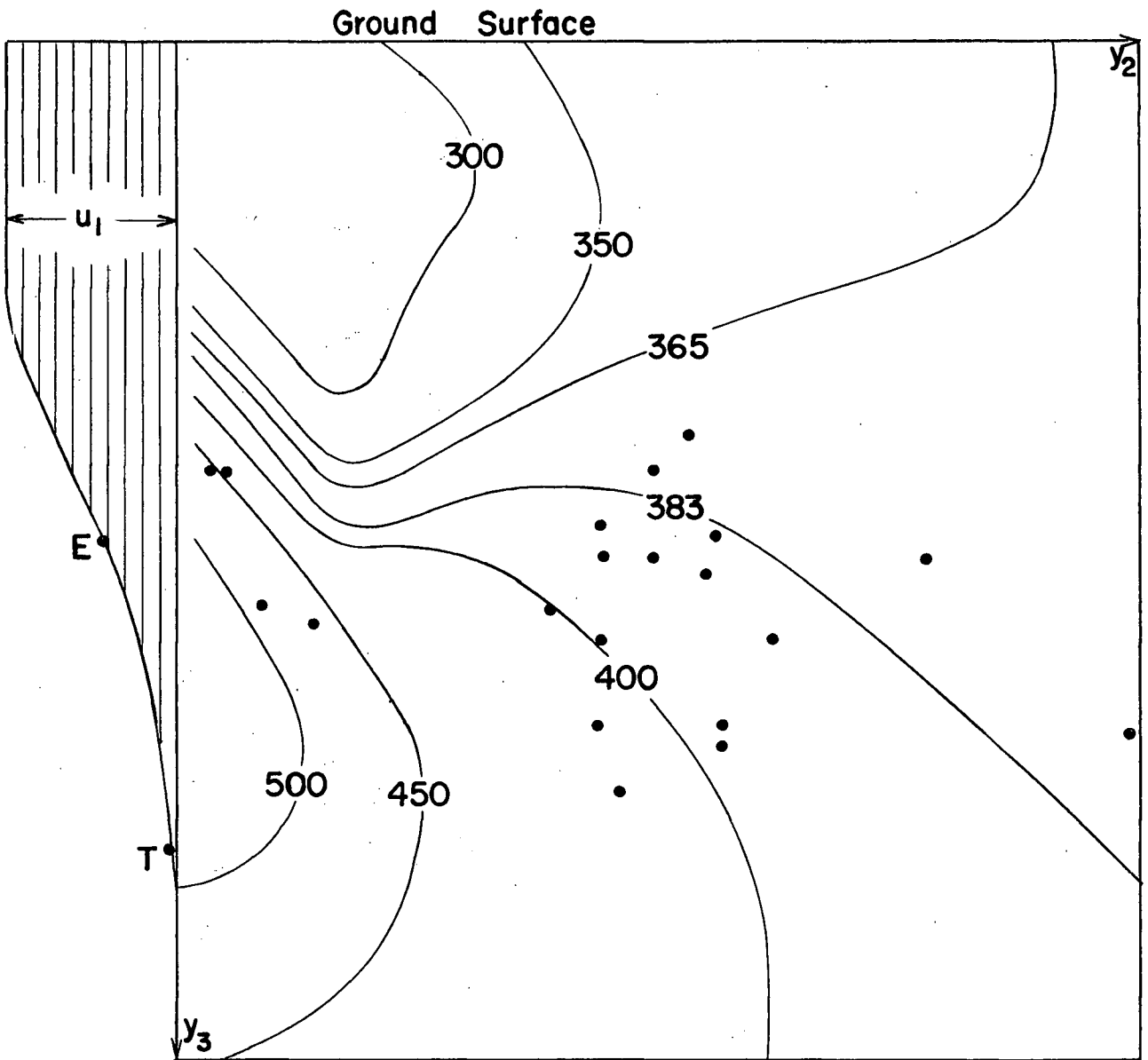


Figure 5.4

Contour map of the magnitude of the maximum shear stress in the vertical plane $y_1 = 0.95L$. Contour units are 10^7 dynes/cm².

Stress release $\tau_{12}^0 = 3.83 \times 10^7$ dynes/cm²

Model D

$d = 0$

$U = 10$ m

$E = 30$ km

$T = 46$ km

$L = 325$ km

$\mu = 3 \times 10^{11}$ cgs

this stress build up in the form of aftershock activity. As a result, all the aftershocks would be expected to lie within the highly stressed region about the fault base. It is quite evident that this proposal does not apply to the geodetic situation shown in figure 5.3 ($y_1 = 0$) where approximately one-third of the hypocentres are located within the highly stressed region. However, this is not the case in the plane $0.95L$ where about 80% of the aftershocks lie in the desired position (figure 5.4).

There are several probable explanations why the aftershock hypocentres do not all lie in the highly stressed region. Indeed, the fault may not be of the strike-slip variety. This is indicated by the fact that fewer aftershocks appear on one side of the main epicentre than on the other i.e. the region to the north-east (figure 5.2) appears to be in compression while that to the south-west appears to be in tension. A situation similar to this arose from the Alaskan earthquake of March 27, 1964 (Plafker, 1965) where vertical displacements of up to 10m were measured.

If the same explanation does not apply to the Rat Island earthquake, then the fault must extend well beyond the aftershock zone and exhibit both a

variable horizontal as well as a variable vertical slip. A horizontal slip of teardrop shape would be a reasonable discontinuity (Chinnery, private communication) since it would represent a large displacement in the region near the main epicentre which would diminish with distance from the initial shock. It is also evident by comparing figures 5.3 and 5.4 that dislocation theory supports this proposal - most of the aftershocks lie in the region of high stress only near the end of the fault (figure 5.4) and not its central plane (figure 5.3). This would also indicate that the aftershock sequence could be associated with the stress released when the fracture extends itself lengthwise. Any definite conclusions in this respect, however, would require a considerable amount of work including the reconstruction of the specific equations for the displacement field and stress changes.

CHAPTER 6

CONCLUSIONS

Many aspects of geophysics deal with inaccessible areas such as the depths of the interior of the earth, theoretically accessible regions of which are only partially covered by geodetic observations. No mathematical model ever represents reality, yet, given a certain set of assumptions, it is usually possible to establish a very close agreement between theory and observation by varying the parameters. There are usually several models that can be justified theoretically but of these only one approximates reality. The problem of eliminating the multiplicity of possibilities and finding the one model that conforms to all available geodetic data is ideally suited to the modern methods of computer analysis. The computer can accommodate the observations and simulate the processes given by the pertinent equations. It can perform these operations very rapidly, and incorrect solutions that fail to conform to reality can be improved in a reasonable time by amended equations, by new data or by both. These arguments, together with the results of the previous two chapters, indicate that our attempt to represent

the natural processes of faulting, using dislocation theory as a general mathematical model, is reasonable.

The use of Steketee's "Elasticity Theory of Dislocations" restricts our analyses to materials which obey Hooke's Law fairly closely. This indicates that the non-elastic or plastic effects associated with the process of fracture are confined to a comparatively small zone in the immediate vicinity of the fault, and that this zone may be represented by a dislocation surface. The medium, of course, is assumed to consist of a homogeneous isotropic material that is semi-infinite with respect to the fracture zone.

The theory, however, does have limitations other than those mentioned above and those discussed in Chapter 1. The horizontal slip u_1 was assumed to vary only in the vertical and not in the horizontal plane. Also, the stress release at the origin, τ_{12}^0 is strictly a theoretical approximation. No physical measurements of this fracture-causing stress have ever been made. Hence, it is impossible to account for the reasons of the initial fracture and the magnitude of the stress that cause it.

Nevertheless, as long as we consider these limitations in our interpretation of the numerical results, we are justified in expecting the theory to provide much information about the displacement field and stress changes produced by fracturing. Such knowledge allows us to estimate the depth of a given fracture and to examine the contours of the maximum shear stress in the disturbed region i.e. it allows us to predict a plausible aftershock sequence associated with a new fracture zone. Possibly, this approach can be developed further so that the foreshock sequence and the prediction of earthquakes may be facilitated.

Finally, there is an extension of the theory which may be of special interest viz. the consideration of a dislocation surface that exhibits both variable vertical and horizontal slip. With the theory allowing for both of these features, the analytical results might be able to suggest a possible connection between strike-slip faulting and mountain building (Chinnery, 1965). If such a relationship could be substantiated by actual geological features, the importance of the use of dislocation theory in association with tectonic changes in the earth's crust would be fully realized.

APPENDIX

THE EVALUATION OF THE DISPLACEMENT FIELD
AND THE STRESS CHANGES

We have to determine the displacement field u_k and the stress changes τ_{ij} at points $P(y_1, y_2, y_3)$ due to a distribution of nuclei at points $Q(x_1, 0, x_3)$ on the dislocation surface shown in figure

2.1. The resulting algebra is very involved and tedious. To simplify the expressions, the following terms will be used,

$$p = x_3 + y_3$$

$$q = x_3 - y_3$$

$$t = x_1 - y_1$$

$$s_1^2 = t^2 + y_2^2 + q^2$$

$$s_2^2 = t^2 + y_2^2 + p^2$$

Table A.1 contains an array of expressions that undergo specific transformations when differentiated with respect to y_i ($i = 1, 2, 3$). In particular we find the following three relationships,

$$\frac{\partial Z_k}{\partial y_1} = t A_k$$

$$\frac{\partial Z_k}{\partial y_2} = -y_2 A_k$$

$$\frac{\partial Z_k}{\partial y_3} = -Z_{k+1}$$

which are valid for both starred and non-starred values of Z, A, B, and C. A second table (A.2) has also been constructed to illustrate a similar set of transformations. In this case two basic relationships exist for both starred and non-starred values of I, J, K, and L, viz.:

$$\frac{\partial I_k}{\partial y_1} = I_{k+1}$$

$$\frac{\partial I_k}{\partial y_2} = -y_2 J_k$$

The following two relationships are also applicable to table (A.2),

$$\frac{\partial I_k}{\partial y_3} = -p J_k$$

$$\frac{\partial I_k^*}{\partial y_3} = q J_k$$

A. THE DISPLACEMENT FIELD

From equations (2.12), u_k is given by

$$u_k = \Gamma_{k,ii} - \frac{2}{3} \Gamma_{i,ik} \quad (1)$$

$$\Gamma_k = \frac{1}{8\pi\mu} \int_{-L}^L \int_d^D \Gamma_{12}^k u_i(x_3) dx_1 dx_3 \quad (2)$$

The Galerkin vector Γ_{12}^k for a nucleus at the point $(x_1, 0, x_3)$ is given by the following expressions:

$$\begin{aligned} \Gamma_{12}^1 &= -\mu y_2 \left(\frac{1}{s_1} + \frac{1}{s_2} \right) \\ \Gamma_{12}^2 &= \mu t \left(\frac{1}{s_1} + \frac{1}{s_2} \right) \end{aligned} \quad (3)$$

and

$$\Gamma_{12}^3 = \frac{\mu t y_2}{(s_2 + p)^2} \left[2c - \frac{2(bp+q)}{s_2} - \frac{(p^2 - q^2)(2s_2 + p)}{s_2^3} \right]$$

where $b = \frac{\lambda - \mu}{\lambda + \mu}$ and $c = \frac{\mu \lambda}{(\lambda + \mu)^2}$ which reduce to $b = 0$ and $c = 1/4$ on the assumption that

$$\lambda = \mu$$

We now define a term ϵ_k such that

TABLE (I) OF RELATIONSHIPS

$Z_1 =$	$A_1 = -\frac{1}{2} \ln(s_2+p) - \frac{p}{2(s_2+p)}$	$B_1 = \frac{1}{2(s_2+p)^2}$	$C_1 = \frac{1}{s_2(s_2+p)^3}$
$Z_2 = -s_2 + p \ln(s_2+p)$	$A_2 = \frac{1}{s_2+p}$	$B_2 = \frac{1}{s_2(s_2+p)^2}$	$C_2 = \frac{3s_2+p}{s_2^3(s_2+p)^3}$
$Z_3 = -\ln(s_2+p)$	$A_3 = \frac{1}{s_2(s_2+p)}$	$B_3 = \frac{2s_2+p}{s_2^3(s_2+p)^2}$	$C_3 = \frac{8s_2^2+9ps_2+3p^2}{s_2^5(s_2+p)^3}$
$Z_4 = \frac{1}{s_2}$	$A_4 = \frac{1}{s_2^3}$	$B_4 = \frac{3}{s_2^5}$	$C_4 = \frac{15}{s_2^7}$
$Z_5 = \frac{p}{s_2^3}$	$A_5 = \frac{3p}{s_2^5}$	$B_5 = \frac{15p}{s_2^7}$	$C_5 = \frac{105p}{s_2^9}$
$Z_6 = \frac{3p^2 - s_2^2}{s_2^5}$	$A_6 = \frac{3(5p^2 - s_2^2)}{s_2^7}$	$B_6 = \frac{15(7p^2 - s_2^2)}{s_2^9}$	$C_6 = \frac{105(9p^2 - s_2^2)}{s_2^{11}}$
$Z_1^* =$	$A_1^* = -\frac{1}{2} \ln(s_1+q) - \frac{q}{2(s_1+q)}$	$B_1^* = \frac{1}{2(s_1+q)^2}$	$C_1^* = \frac{1}{s_1(s_1+q)^3}$
$Z_2^* = s_1 - q \ln(s_1+q)$	$A_2^* = \frac{-1}{s_1+q}$	$B_2^* = \frac{-1}{s_1(s_1+q)^2}$	$C_2^* = \frac{-(3s_1+q)}{s_1^3(s_1+q)^3}$
$Z_3^* = -\ln(s_1+q)$	$A_3^* = \frac{1}{s_1(s_1+q)}$	$B_3^* = \frac{2s_1+q}{s_1^3(s_1+q)^2}$	$C_3^* = \frac{8s_1^2+9qs_1+3q^2}{s_1^5(s_1+q)^3}$
$Z_4^* = -\frac{1}{s_1}$	$A_4^* = -\frac{1}{s_1^3}$	$B_4^* = -\frac{3}{s_1^5}$	$C_4^* = -\frac{15}{s_1^7}$
$Z_5^* = \frac{q}{s_1^3}$	$A_5^* = \frac{3q}{s_1^5}$	$B_5^* = \frac{15q}{s_1^7}$	$C_5^* = \frac{105q}{s_1^9}$
$Z_6^* = \frac{-(3q^2 - s_1^2)}{s_1^5}$	$A_6^* = \frac{3(s_1^2 - 5q^2)}{s_1^7}$	$B_6^* = \frac{-15(7q^2 - s_1^2)}{s_1^9}$	$C_6^* = \frac{-105(9q^2 - s_1^2)}{s_1^{11}}$
In the above table operations of the following form are valid: $\frac{\partial A_i}{\partial y_1} = tB_i$; $\frac{\partial A_i^*}{\partial y_1} = tB_i^*$; $\frac{\partial A_i}{\partial y_2} = -y_2 B_i$; $\frac{\partial A_i^*}{\partial y_2} = -y_2 B_i^*$; $\frac{\partial A_i}{\partial y_3} = -A_{i+1}$; $\frac{\partial A_i^*}{\partial y_3} = -A_{i+1}^*$			

TABLE A.I.

TABLE (II) OF RELATIONSHIPS

$I_1 =$	$J_1 = \frac{1}{2} \ln(s_2+t) - \frac{t}{2(s_2+t)}$	$K_1 = \frac{1}{2(s_2+t)^2}$	$L_1 = \frac{1}{s_2(s_2+t)^3}$
$I_2 = -s_2 + t \ln(s_2+t)$	$J_2 = \frac{1}{s_2+t}$	$K_2 = \frac{1}{s_2(s_2+t)^2}$	$L_2 = \frac{3s_2+t}{s_2^3(s_2+t)^3}$
$I_3 = -\ln(s_2+t)$	$J_3 = \frac{1}{s_2(s_2+t)}$	$K_3 = \frac{2s_2+t}{s_2^3(s_2+t)^2}$	$L_3 = \frac{8s_2^2+9ts_2+3t^2}{s_2^5(s_2+t)^3}$
$I_4 = \frac{1}{s_2}$	$J_4 = \frac{1}{s_2^3}$	$K_4 = \frac{3}{s_2^5}$	$L_4 = \frac{15}{s_2^7}$
$I_5 = \frac{t}{s_2^3}$	$J_5 = \frac{3t}{s_2^5}$	$K_5 = \frac{15t}{s_2^7}$	$L_5 = \frac{105t}{s_2^9}$
$I_6 = \frac{3t^2 - s_2^2}{s_2^5}$	$J_6 = \frac{3(5t^2 - s_2^2)}{s_2^7}$	$K_6 = \frac{15(7t^2 - s_2^2)}{s_2^9}$	$L_6 = \frac{105(9t^2 - s_2^2)}{s_2^{11}}$
$I_1^* =$	$J_1^* = \frac{1}{2} \ln(s_1+t) - \frac{t}{2(s_1+t)}$	$K_1^* = \frac{1}{2(s_1+t)^2}$	$L_1^* = \frac{1}{s_1(s_1+t)^3}$
$I_2^* = -s_1 + t \ln(s_1+t)$	$J_2^* = \frac{1}{s_1+t}$	$K_2^* = \frac{1}{s_1(s_1+t)^2}$	$L_2^* = \frac{2s_1+t}{s_1^3(s_1+t)^3}$
$I_3^* = -\ln(s_1+t)$	$J_3^* = \frac{1}{s_1(s_1+t)}$	$K_3^* = \frac{2s_1+t}{s_1^3(s_1+t)^2}$	$L_3^* = \frac{8s_1^2+9ts_1+3t^2}{s_1^5(s_1+t)^3}$
$I_4^* = \frac{1}{s_1}$	$J_4^* = \frac{1}{s_1^3}$	$K_4^* = \frac{3}{s_1^5}$	$L_4^* = \frac{15}{s_1^7}$
$I_5^* = \frac{t}{s_1^3}$	$J_5^* = \frac{3t}{s_1^5}$	$K_5^* = \frac{15t}{s_1^7}$	$L_5^* = \frac{105t}{s_1^9}$
$I_6^* = \frac{3t^2 - s_1^2}{s_1^5}$	$J_6^* = \frac{3(5t^2 - s_1^2)}{s_1^7}$	$K_6^* = \frac{15(7t^2 - s_1^2)}{s_1^9}$	$L_6^* = \frac{105(9t^2 - s_1^2)}{s_1^{11}}$

In the above table operations of the following form are valid: $\frac{\partial J_i}{\partial y_1} = J_{i+1}$; $\frac{\partial J_i^*}{\partial y_1} = J_{i+1}^*$; $\frac{\partial J_i}{\partial y_2} = -y_2 K_i$; $\frac{\partial J_i^*}{\partial y_2} = -y_2 K_i^*$; $\frac{\partial J_i}{\partial y_3} = -p K_i$; $\frac{\partial J_i^*}{\partial y_3} = q K_i^*$

TABLE A.2

$$\epsilon_k = \int_{-L}^L \Gamma_{12}^k dx_1 \quad (4)$$

This implies that the displacement field u_k can be expressed as

$$u_k = \frac{1}{8\pi\mu} \int_D u_1(x_3) \omega_k dx_3$$

where

$$\omega_k = \epsilon_{k,li} - \frac{2}{3} \epsilon_{i,ik} \quad (5)$$

1. The components ϵ_k

From equation (A.4) we have

$$\begin{aligned} \epsilon_1 &= \int_{-L}^L \Gamma_{12}^1 dx_1 \\ &= \mu y_2 \int_{-L}^L (z_4^* - z_4) dx_1 \\ &= -\mu y_2 \left[\ln(s_1+t) + \ln(s_2+t) \right] \end{aligned} \quad (6)$$

$$\begin{aligned} \epsilon_2 &= \int_{-L}^L \Gamma_{12}^2 dx_1 \\ &= \mu \int_{-L}^L t (z_4 - z_4^*) dx_1 \\ &= \mu (s_1 + s_2) \end{aligned} \quad (7)$$

and

$$\begin{aligned}
 \epsilon_3 &= \int_{-L}^L \Gamma_{12}^3 dx_1 \\
 &= \mu y_2 \int_{-L}^L t (B_1 - 2q B_2 - 4x_3 y_3 B_3) dx_1 \\
 &= \mu y_2 (-A_1 + 2q A_2 + 4x_3 y_3 A_3) \parallel
 \end{aligned}
 \tag{8}$$

where $f(x_1, 0, x_3) \parallel = f(L, 0, x_3) - f(-L, 0, x_3)$ whenever the symbol \parallel appears.

2. The derivatives of ϵ_κ

We shall now proceed to evaluate the derivatives $\epsilon_{\kappa,ii}$ and $\epsilon_{i,ik}$ which are required in equation (A.5b).

a) The ϵ_1 component

$$\begin{aligned}
 \epsilon_{1,1} &= \mu y_2 (Z_4 - Z_4^*) \parallel \\
 \epsilon_{1,11} &= \mu y_2 t (A_4 - A_4^*) \parallel \\
 \epsilon_{1,2} &= -\mu \left[\ln(s_1+t)(s_2+t) + y_2^2 (J_3 + J_3^*) \right] \parallel \tag{9} \\
 \epsilon_{1,22} &= \mu y_2 \left[-3(J_3 + J_3^*) + y_2^2 (L_1 + L_1^* + J_3^2 + J_3^{*2}) \right] \parallel \\
 \epsilon_{1,3} &= \mu y_2 (q J_3^* - p J_3) \parallel \\
 \epsilon_{1,33} &= \mu y_2 \left[p^2 (A_4 J_2 + J_3^*) + q^2 (J_3^{*2} - A_4^* J_2^*) - (J_3 + J_3^*) \right] \parallel \\
 \nabla^2 \epsilon_1 &= -2 \mu y_2 (J_3 + J_3^*) \parallel
 \end{aligned}$$

b) The ϵ_2 component

$$\begin{aligned}
 \epsilon_{2,1} &= -\mu t (Z_4 - Z_4^*) \parallel \\
 \epsilon_{2,11} &= \mu [(Z_4 - Z_4^*) - t^2(A_4 - A_4^*)] \parallel \\
 \epsilon_{2,2} &= \mu y_2 (Z_4 - Z_4^*) \parallel \\
 \epsilon_{2,22} &= \mu [Z_4 - Z_4^* - y_2^2 (A_4 - A_4^*)] \parallel \\
 \epsilon_{2,3} &= \mu [pZ_4 - qZ_4^*] \parallel \\
 \epsilon_{2,33} &= \mu [A_4 (s_2^2 - p^2) - A_4^* (s_1^2 + q^2)] \parallel \\
 \nabla^2 \epsilon_2 &= 2\mu (Z_4 - Z_4^*) \parallel
 \end{aligned} \tag{10}$$

c) The ϵ_3 component

$$\begin{aligned}
 \epsilon_{3,1} &= \mu y_2 t (-B_1 + 2qB_2 + 4x_3 y_3 B_3) \parallel \\
 \epsilon_{3,11} &= \mu y_2 [t^2(-C_1 + 2qC_2 + 4x_3 y_3 C_3) - (-B_1 + 2qB_2 + 4x_3 y_3 B_3)] \parallel \\
 \epsilon_{3,2} &= \mu [-A_1 + 2qA_2 + 4x_3 y_3 A_3 - y_2^2 (-B_1 + 2qB_2 + 4x_3 y_3 B_3)] \parallel \\
 \epsilon_{3,22} &= \mu y_2 [-3(-B_1 + 2qB_2 + 4x_3 y_3 B_3) + y_2^2 (-C_1 + 2qC_2 + 4x_3 y_3 C_3)] \parallel \\
 \epsilon_{3,3} &= \mu y_2 (-A_2 + 2pA_3 - 4x_3 y_3 A_4) \parallel \\
 \epsilon_{3,33} &= \mu y_2 [3A_3 - 2A_4(p + 2x_3) + 4x_3 y_3 A_5] \parallel \\
 \nabla^2 \epsilon_3 &= 4\mu y_2 (A_3 - 2x_3 A_4) \parallel
 \end{aligned}$$

d) The divergence $\epsilon_{\kappa, \kappa}$

$$\begin{aligned} \operatorname{div} \epsilon &= \epsilon_{1,1} + \epsilon_{2,2} + \epsilon_{3,3} \\ &= \mu y_2 \left[2(Z_4 - Z_4^*) - A_2 + 2pA_3 - 4x_3 y_3 A_4 \right] \end{aligned} \quad (12)$$

e) The term $\operatorname{Grad}_{\kappa} (\operatorname{div} \epsilon)$

$$\begin{aligned} \operatorname{Grad}_1 (\operatorname{div} \epsilon) &= \mu y_2 t (2A_4 - 2A_4^* - B_2 + 2pB_3 - 4x_3 y_3 B_4) \\ \operatorname{Grad}_2 (\operatorname{div} \epsilon) &= \mu \left[A_2 - 2Z_4^* + 4pA_3 - 4x_3 y_3 A_4 - y_2^2 (B_2 - 2A_4^* + 4pB_3 - 4x_3 y_3 B_4) \right] \\ \operatorname{Grad}_3 (\operatorname{div} \epsilon) &= \mu y_2 \left[2Z_5^* - 2Z_5 + 3A_3 - 2A_4 (p + 2x_3) + 4x_3 y_3 A_5 \right] \end{aligned} \quad (13)$$

3. The formulation of the terms ω_{κ}

We can now determine the expressions ω_{κ} by applying the results of the previous section (appendix A.2) to equation (A.5b). The resulting terms are

$$\begin{aligned} \omega_1 &= \left[-2\mu y_2 (J_3 + J_3^*) - \frac{2}{3} \mu y_2 t (A_4 + 3pB_3 - 2A_4^* - 4x_3 y_3 B_4) \right] \\ \omega_2 &= \mu \left[2(Z_4 + Z_4^*) - \frac{2}{3} (A_2 - 2Z_4^* + 4pA_3 - 4x_3 y_3 A_4) \right. \\ &\quad \left. + \frac{2}{3} y_2^2 (A_4 + 3pB_3 - 2A_4^* - 4x_3 y_3 B_4) \right] \end{aligned}$$

and

$$\omega_3 = \frac{2}{3} \mu y_2 \left[3A_3 + 2A_4(y_3 - 3x_3) - 4x_3 y_3 A_5 + 2(Z_5 - Z_5^*) \right] \parallel \quad (14)$$

For the sake of brevity, it is advantageous to define four new expressions, viz.:

$$F_1 = J_3 + J_3^* \parallel$$

$$F_2 = A_4 - 2A_4^* + 3\rho B_3 - 4x_3 y_3 B_4 \parallel \quad (15)$$

$$F_3 = 2A_2 - Z_4^* - \rho A_3 + 4x_3 y_3 A_4 \parallel$$

$$F_4 = 3A_3 + 2A_4(y_3 - 3x_3) - 4x_3 y_3 A_5 + 2(Z_5 - Z_5^*) \parallel$$

4. The actual displacement fields

By substituting the expressions for ω_1, ω_2 and ω_3 into equation (A.5a) we obtain the three displacements

$$\begin{aligned} u_1 &= -\frac{1}{4\pi} \int_d^D u_1(x_3) y_2 \left(F_1 + \frac{t}{3} F_2 \right) dx_3 \\ u_2 &= \frac{1}{12\pi} \int_d^D u_1(x_3) (F_3 + y_2^2 F_2) dx_3 \end{aligned} \quad (16)$$

and

$$u_3 = \frac{1}{12\pi} \int_d^D u_1(x_3) y_2 F_4 dx_3$$

which can be evaluated very easily with the aid of an electronic computer (an I.B.M. 7040 was used in our case).

B. THE STRESS CHANGES

From equation (2.17), the changes in stress are given by

$$\tau_{ij} = \frac{1}{8\pi} \int_d^D u_1(x_3) (\delta_{ij} \omega_{k,k} + \omega_{i,j} + \omega_{j,i}) dx_3 \quad (1)$$

We shall now evaluate the derivatives $\omega_{k,k}$, $\omega_{i,j}$ and $\omega_{j,i}$ which are required to formulate these equations explicitly.

1. The derivatives of ω_k

a) The ω_1 component

$$\omega_{1,1} = -\frac{2}{3} \mu y_2 \left[3(J_4 + J_4^*) - A_4 + 2A_4^* - 3p B_3 + 4x_3 y_3 B_4 + t^2 (B_4 - 2B_4^* + 3p C_3 - 4x_3 y_3 C_4) \right] \parallel$$

$$\omega_{1,2} = -2\mu \left[J_3 + J_3^* - y_2^2 (K_3 + K_3^*) \right] \quad (2)$$

$$+ \frac{t}{3} \left\{ (A_4 - 2A_4^* + 3p B_3 - 4x_3 y_3 B_4) - y_2^2 (B_4 - 2B_4^* + 3p C_3 - 4x_3 y_3 C_4) \right\} \parallel \parallel$$

$$\omega_{1,3} = 2\mu y_2 \left[p K_3 - q K_3^* - \frac{t}{3} (-A_5 + 2A_5^* + 3B_3 - B_4 (3p + 4x_3) + 4x_3 y_3 B_5) \right] \parallel$$

b) The ω_2 component

$$\omega_{2,1} = \frac{2}{3} \mu t \left[2B_2 - A_4^* - pB_3 + 4x_3y_3B_4 + y_2^2 (B_4 - 2B_4^* + 3pC_3 - 4x_3y_3C_4) \right] \parallel$$

$$\omega_{2,2} = -\frac{2}{3} \mu y_2 \left[2B_2 - A_4^* - pB_3 + 4x_3y_3B_4 - 2(A_4 - 2A_4^* + 3pB_3 - 4x_3y_3B_4) + y_2^2 (B_4 - 2B_4^* + 3pC_3 - 4x_3y_3C_4) \right] \parallel \quad (3)$$

$$\omega_{2,3} = \frac{2}{3} \mu \left[Z_5^* - 3A_3 + A_4(p + 4x_3) - 4x_3y_3A_5 + y_2^2 (2A_5^* - A_5 + 3B_3 - B_4(3p + 4x_3) + 4x_3y_3B_5) \right] \parallel$$

c) The ω_3 component

$$\omega_{3,1} = \frac{2}{3} \mu y_2 t \left[3B_3 + 2B_4(y_3 - 3x_3) - 4x_3y_3B_5 - 2A_5^* + 2A_5 \right] \parallel$$

$$\omega_{3,2} = \frac{2}{3} \mu \left[3A_3 + 2A_4(y_3 - 3x_3) - 4x_3y_3A_5 + 2(Z_5 - Z_5^*) - y_2^2 (3B_3 + 2B_4(y_3 - 3x_3) - 4x_3y_3B_5 + 2(A_5 - A_5^*)) \right] \parallel \quad (4)$$

$$\omega_{3,3} = \frac{2}{3} \mu y_2 \left[-A_4 + 2qA_5 + 4x_3y_3A_6 + 2(Z_6 - Z_6^*) \right] \parallel$$

2. The grouping of specific terms

a) The divergence

$$\begin{aligned} \operatorname{div} \omega &= \omega_{1,1} + \omega_{2,2} + \omega_{3,3} \\ &= -\frac{4}{3} \mu y_2 (2A_4 - A_4^* - 2x_3 A_5) \parallel \parallel \quad (5) \end{aligned}$$

b) The symmetric sums

$$\begin{aligned} \omega_{2,1} + \omega_{1,2} &= -\frac{2}{3} \mu \left[3(J_3 + J_3^*) - 3y_2^2 (K_3 + K_3^*) \right. \\ &\left. - 2t y_2^2 (B_4 - 2B_4^* + 3pC_3 - 4x_3 y_3 C_4 - t(6B_2 - 5A_4 + 8x_3 y_3 B_4 + A_4^*)) \right] \parallel \parallel \end{aligned}$$

$$\omega_{3,1} + \omega_{1,3} = \frac{2}{3} \mu y_2 \left[3(pk_3 - qk_3^*) \right. \quad (6)$$

$$\left. - 4t(A_5^* + 2x_3 y_3 B_5 - B_4(x_3 + 2y_3)) \right] \parallel \parallel$$

$$\omega_{3,2} + \omega_{2,3} = \frac{2}{3} \mu \left[-Z_5^* + A_4(x_3 + 5y_3) - 8x_3 y_3 A_5 \right.$$

$$\left. + 4y_2^2 (A_5^* + 2x_3 y_3 B_5 - B_4(x_3 + 2y_3)) \right] \parallel \parallel$$

3. The actual stress changes

Substituting the equations of appendix (B.2) above into equation (B.1) we obtain the six components

of the stress change

$$\begin{aligned}\tau_{11} &= \frac{1}{8\pi} \int_d^D u_1(x_3) (\operatorname{div} \omega + 2 \omega_{1,1}) dx_3 \\ \tau_{22} &= \frac{1}{8\pi} \int_d^D u_1(x_3) (\operatorname{div} \omega + 2 \omega_{2,2}) dx_3 \\ \tau_{33} &= \frac{1}{8\pi} \int_d^D u_1(x_3) (\operatorname{div} \omega + 2 \omega_{3,3}) dx_3 \\ \tau_{12} &= \frac{1}{8\pi} \int_d^D u_1(x_3) (\omega_{1,2} + \omega_{2,1}) dx_3 \\ \tau_{13} &= \frac{1}{8\pi} \int_d^D u_1(x_3) (\omega_{1,3} + \omega_{3,1}) dx_3 \\ \tau_{23} &= \frac{1}{8\pi} \int_d^D u_1(x_3) (\omega_{2,3} + \omega_{3,2}) dx_3\end{aligned}\tag{7}$$

Analytical solutions can easily be obtained for each of these expressions with the aid of an electronic computer (an I.B.M. 7040 was used to perform this task).

C. THE MAXIMUM SHEAR STRESS

Having evaluated equations (B.7) at any given point we may calculate the principal stresses and hence the maximum shear stress at that point. Equation (2.20),

$$|\tau_{ij} - \tau \delta_{ij}| = 0 \tag{1}$$

yields a cubic equation of the form

$$-\tau^3 + \textcircled{H}_1 \tau^2 - \textcircled{H}_2 \tau + \textcircled{H}_3 = 0 \tag{2}$$

where \textcircled{H}_1 , \textcircled{H}_2 and \textcircled{H}_3 are invariants of the stress tensor and are described by the following equations:

$$\begin{aligned} \textcircled{H}_1 &= \tau_1 + \tau_2 + \tau_3 \\ &= \tau_{11} + \tau_{22} + \tau_{33} \end{aligned}$$

$$\begin{aligned} \textcircled{H}_2 &= \tau_1 \tau_2 + \tau_2 \tau_3 + \tau_3 \tau_1 \\ &= \begin{vmatrix} \tau_{22} & \tau_{23} \\ \tau_{23} & \tau_{33} \end{vmatrix} + \begin{vmatrix} \tau_{11} & \tau_{31} \\ \tau_{31} & \tau_{33} \end{vmatrix} + \begin{vmatrix} \tau_{11} & \tau_{12}^{(*)} \\ \tau_{12}^{(*)} & \tau_{22} \end{vmatrix} \end{aligned}$$

and

$$\Theta_3 = \tau_1 \tau_2 \tau_3$$

$$= \begin{vmatrix} \tau_{11} & \tau_{12}^{(*)} & \tau_{13} \\ \tau_{12}^{(*)} & \tau_{22} & \tau_{23} \\ \tau_{13} & \tau_{23} & \tau_{33} \end{vmatrix}$$

(3)

Here τ_1 , τ_2 and τ_3 are the three roots of the cubic equation such that $\tau_3 > \tau_2 > \tau_1$. The maximum shear stress is given by

$$|S_{\max}| = \frac{\tau_3 - \tau_1}{2}$$

(4)

For the reasons mentioned in Chapter 2.7 no reference will be made to the directions of maximum shear stress. However, it is important to note that when an initial stress distribution τ_{12}° exists in the medium, it must be added to the stress change given by equation (B.7d). Thus in our case all the τ_{12} terms in equations (C.3) are of the form

$$\tau_{12}^* = \tau_{12} + \tau_{12}^{\circ}$$

(5)

REFERENCES

- Anderson, E. M., Dynamics of Faulting, 2nd ed., Oliver and Boyd, Edinburgh, 1951.
- Badgley, P. C., Structural Methods for the Exploration Geologist, Harper and Bros., New York, 1959.
- Ben-Menahem, A. and Tokso, M. N., Source Mechanism from Spectra of Long-period Seismic Surface Waves, J. Geophys. Res., 67, 1943-1955, 1962.
- Ben-Menahem, A. and Tokso, M. N., Source Mechanism for Spectrums of Long-period Surface Waves, J. Geophys. Res., 68, 5207-5222, 1963.
- Benioff, H., Mechanism of Earthquake Generation, Bull. Geol. Soc. Amer., 62, 1526, 1951a.
- Benioff, H., Earthquakes and Rock Creep, Part I: Creep characteristics of Rocks and the Origin of Aftershocks, Bull. Seism. Soc. Amer., 41, 31-62, 1951b.
- Benioff, H. and Gutenberg, B., "Strain Characteristics of the Earth's Interior" in Internal Constitution of the Earth, Dover Publications, New York, 382-407, 1951.
- Benioff, H., Mechanism and Strain Characteristics of the White Wolf Fault as Indicated by the Aftershock Sequence, Calif. Div. Mines Bull., 171, 199-202, 1955.
- Bilby, B. A., "Continuous Distribution of Dislocations" in Progress in Solid Mechanics, 1, North Holland Publishing Co., 1960.
- Burgess, J. M., Proc. Kon. Ned. Acad. Wetensch, 42, 293 and 378, 1939.
- Byerly, P. and De Noyer, J., "Contributions in Geophysics in Honor of Beno Gutenberg" in International Series of Monographs on Earth Sciences, 17-35, 1958.

- Byerly, P., Slemmons, D. B., Tocher, D., Steinbrugge, K. V., Moran, D. F., and Cloud, W. K., The Fallon-Stillwater Earthquakes of July 6, 1954 and August 23, 1954, Bull. Seism. Soc. Amer., 46, 1-40, 1956.
- Chinnery, M. A., The Application of Dislocation Theory to Geodynamics, M. A. Thesis, University of Toronto, 1959.
- Chinnery, M. A., Some Physical Aspects of Earthquake Mechanism, J. Geophys. Res., 65, 3852-3854, 1960.
- Chinnery, M. A., The Deformation of the Ground around Surface Faults, Bull. Seism. Soc. Amer., 51, 355-372, 1961.
- Chinnery, M. A., The Dynamics of the Strike-slip Fault, Ph.D. Thesis, University of Toronto, 1962.
- Chinnery, M. A., The Stress Changes that Accompany Strike-slip Faulting, Bull. Seism. Soc. Amer., 53, 921-932, 1963.
- Chinnery, M. A., The Strength of the Earth's Crust under Horizontal Shear Stress, J. Geophys. Res., 69, 2085-2089, 1964.
- Chinnery, M. A., The Vertical Displacements Associated with Transcurrent Faulting, J. Geophys. Res., 70, 4627-4632, 1965.
- Galerkin, B., Comp. Rend. Acad. Sci., U.S.S.R., 353, 1930.
- Griffith, A. A., The Phenomena of Rupture and Flow in Solids, Phil. Trans. Roy. Soc. London, A, 221, 163-197, 1921.
- Griffith, A. A., Theory of Rupture, First International Congress of Appl. Mech., Delft, 55-63, 1924.
- Gutenberg, B. and Richter, C. F., Earthquake Magnitude, Energy and Acceleration, Bull. Seism. Soc. Amer., 32, 163-191, 1942.
- Gutenberg, B. and Richter, C. F., Earthquake Magnitude, Intensity, Energy, and Acceleration, Bull. Seism. Soc. Amer., 46, 105-145, 1956.

- Hafner, W., Shear Distribution and Faulting, Bull. Geol. Soc. Amer. 62, 373-398, 1951.
- Handin, J., Flow, Fracture, and Strength of Rocks in the Laboratory, Trans. Am. Geophys. Union, 41, 162-165, 1960.
- Inglis, C. E., Stress in a Plate due to the Presence of Cracks and Sharp Corners, Proc. Inst. Nav. Arch., 55, 219-230, 1913.
- Jacobs, J. A., The Earth's Core and Geomagnetism, The MacMillan Company, New York, 1963.
- Jordan, J. N. and Lander, J. F., Aftershocks of the 4 February 1965 Rat Island Earthquake, Science, 148, 1323-1325, 1965.
- Kasahara, K., The Nature of Seismic Origins as Inferred from Seismological and Geodetic Observations (1), Bull. Earth. Res. Inst., 35, 473-532, 1957.
- Kasahara, K., Physical Conditions of Earthquake Faults as Deduced from Geodetic Data, Bull. Earth. Res. Inst., 36, 455-464, 1958a.
- Kasahara, K., Fault Origin Model of Earthquakes, with Special Reference to the Tango Earthquake, 1927, J. Phys. Earth, 6, 1, 15-22, 1958b.
- Kasahara, K., Physical Conditions of Earthquake Faults (II). A Model of Strike-slip faults with Various Dip Angles, Bull. Earth. Res. Inst., 37, 39-51, 1959.
- Knopoff, L., Energy Release in Earthquakes, Geophys. J., 1, 44-52, 1958.
- Ladner, J. F., Seismological Notes - January and February 1965, Bull. Seism. Soc. Amer., 55, 655-660, 1965.
- Love, A. E. H., Mathematical Theory of Elasticity, 4th ed., Dover Publications, New York, 1944.
- Nadai, A., Theory of Flow and Fracture of Solids, 2nd ed., McGraw-Hill, New York, 1950.

- Nielsen, K. L., Methods in Numerical Analysis, The Mac-Millan Company, New York, 118-130, 1957.
- Orowan, E., Mechanism of Seismic Faulting, Geol. Soc. Amer. Mem., 323-345, 1960.
- Papcovitch, P. F., Compt. Rend., 195, 513-518 and 754-756, 1932.
- Plafker, G., Tectonic Deformation Associated with the 1964 Alaska Earthquake, Science, 148, 1675-1687, 1965.
- Press, F., Displacements, Strains, and Tilts at Teleseismic Distances, J. Geophys. Res., 70, 2395-2412, 1965.
- Richter, C. F., "Foreshocks and Aftershocks" in Earthquakes in Kern County, California, during 1952, Calif. Div. Mines Bull., 171, 177-197, 1955.
- Richter, C. F., Elementary Seismology, W. H. Freeman and Company, San Francisco and London, 1958.
- Richter, C. F., Allen, C. R., and Nordquist, J. M., The Desert Hot Springs Earthquakes and their Tectonic Environment, Bull. Seism. Soc. Amer., 48, 315-337, 1958.
- Scheidegger, A. E., Rheology of the Earth: the Basic Problem of Geodynamics, Can. J. Phys., 35, 383-397, 1957.
- Sneddon, I. N., The Distribution of Stress in the Neighbourhood of a Crack in an Elastic Solid, Proc. Roy. Soc. London, A, 187, 229-260, 1946.
- Sokolnikoff, I. S., Mathematical theory of Elasticity, 2nd ed., McGraw-Hill Book Co., New York, 1956.
- Steketee, J. A., The Elasticity Theory of Dislocations, Unpublished Report, Dept. App. Math., University of Toronto, 1957.
- Steketee, J. A., On Volterra's Dislocations in a Semi-Infinite Elastic Medium, Can. J. Phys., 36, 192-205, 1958a.

- Steketee, J. A., Some Geophysical Applications of the Elasticity Theory of Dislocations, Can. J. Phys., 36, 1168-1198, 1958b.
- Tsuboi, C., Earthquake Energy, Earthquake Volume, After-shock Area, and Strength of the Earth's Crust, J. Phys. Earth, 4, 63-66, 1956.
- Vacquier, V., Raff, A. D., and Warren, R. E., Horizontal Displacements in the Floor of the Northeastern Pacific Ocean, Bull. Geol. Soc. Amer., 72, 1251-1258, 1961.
- Volterra, V., Ann. Sci. Ecole Norm. Sup., Ser. 3, 24, 401, 1907.
- Wallace, R. E., Geometry of Shearing Stress and its Relation to Faulting, J. Geol., 59, 118-130, 1951.
- Westergaard, H. M., Theory of Elasticity and Plasticity, Harvard University Press, 1952.
- Whitten, C. A., Horizontal Movement in California, Coast and Geodetic Survey, 2, 84-88, 1949.
- Whitten, C. A., Geodetic Measurements in the Dixie Valley Area, Bull. Seism. Soc. Amer., 47, 321-325, 1957.
- Wilson, J. T., Foreshocks and Aftershocks of the Nevada Earthquake December 20, 1932, and the Parkfield Earthquake of June 7, 1934, Bull. Seism. Soc. Amer., 26, 189-194, 1936.